



HAL
open science

New geological and geochronological constraints on the evolution of the Cotacachi - Cuicocha volcanic complex (Ecuador)

Marco Almeida Vaca, Mathilde Bablon, S. Daniel Andrade, Silvana Hidalgo, Xavier Quidelleur, Francisco Vasconez, Anais Vásconez Müller, Pierre Lahitte, Pablo Samaniego

► To cite this version:

Marco Almeida Vaca, Mathilde Bablon, S. Daniel Andrade, Silvana Hidalgo, Xavier Quidelleur, et al.. New geological and geochronological constraints on the evolution of the Cotacachi - Cuicocha volcanic complex (Ecuador). *Journal of South American Earth Sciences*, 2023, 128, pp.104489. 10.1016/j.jsames.2023.104489 . hal-04166917

HAL Id: hal-04166917

<https://hal.science/hal-04166917v1>

Submitted on 1 Dec 2023

HAL is a multi-disciplinary open access archive for the deposit and dissemination of scientific research documents, whether they are published or not. The documents may come from teaching and research institutions in France or abroad, or from public or private research centers.

L'archive ouverte pluridisciplinaire **HAL**, est destinée au dépôt et à la diffusion de documents scientifiques de niveau recherche, publiés ou non, émanant des établissements d'enseignement et de recherche français ou étrangers, des laboratoires publics ou privés.

1 **New geological and geochronological constraints on the evolution of the Cotacachi**
2 **- Cuicocha Volcanic Complex (Ecuador)**

3 *Marco Almeida Vaca¹, Mathilde Bablon^{2,3}, S. Daniel Andrade¹, Silvana Hidalgo¹, Xavier Quidelleur²,*
4 *Francisco J. Vasconez¹, Anais Vásconez Müller¹, Pierre Lahitte², Pablo Samaniego⁴*

5 ¹ *Instituto Geofísico, Escuela Politécnica Nacional, Ap. 17-01-2759, Quito, Ecuador.*

6 ² *Université Paris-Saclay, CNRS, GEOPS, Orsay, 91405, France.*

7 ³ *Université Côte d'Azur, CNRS, IRD, Observatoire de la Côte d'Azur, Géoazur, Valbonne, France*

8 ⁴ *Laboratoire Magmas et Volcans, Université Clermont Auvergne - CNRS - IRD, 6 Avenue Blaise Pascal, 63178*
9 *Aubière, France.*

10 **Abstract**

11 Extensive fieldwork at the Cotacachi-Cuicocha Volcanic Complex (CCVC, North of
12 Ecuador) resulted in a new collection of geological data including cartography,
13 chronology, petrography, geochemistry, and morphology. This volcanic complex is
14 formed by a central volcano (Cotacachi: 4939 m asl, current bulk volume of 56 ± 4
15 km^3), several peripheral domes, and a 3 km wide volcanic caldera (Cuicocha: $4.2 \pm$
16 0.1 km^3). CCVC comprises three stratigraphic members: The first, Cotacachi Basal,
17 represents the initial phase of construction, which started at $173 \pm 4 \text{ ka}$ with a basal
18 andesitic lava flow succession (~500 m-thick) including isolated basaltic-andesitic
19 lavas (Verde Tola unit; NE: $113 \pm 6 \text{ ka}$, SE: $133 \pm 9 \text{ ka}$), the construction of some
20 peripheral amphibole-bearing andesitic domes, such as Muyurcu and Loma Negra
21 ($138 \pm 4 \text{ ka}$ and $<108 \text{ ka}$, respectively), and a debris-avalanche deposit to the north-
22 west ($0.5 - 1.8 \text{ km}^3$, older than 108 ka). The second member, Upper Cotacachi,
23 consists of an andesitic lava flow succession (~300 m-thick), younger than 108 ± 6
24 ka. A gap of activity occurred afterwards from 100 to 70 ka, during which a second
25 debris-avalanche ($0.2 - 1.1 \text{ km}^3$, 108 to 65 ka) occurred to the NE, followed by the
26 effusion of the dacitic Piribuela dome ($65 \pm 2 \text{ ka}$). Afterwards, several superimposed
27 andesitic lava flows were emplaced at the summit, possibly around 15 - 10 ka since
28 they lack glacial erosion. The third member includes the extrusion of the andesitic
29 Cuicocha pre-caldera domes, which marks the beginning of a new eruptive stage of
30 activity of CCVC during the Holocene, resulting in a violent eruption (3525 ± 35 to
31 $2980 \pm 30 \text{ a BP}$; VEI= 5) that partially destroyed the young dome and formed a
32 funnel-shaped caldera (Cuicocha Caldera-Lake), ending with the emplacement of
33 the Wolf and Yerovi post-caldera domes.

34 1. INTRODUCTION

35 The Cotacachi-Cuicocha Volcanic Complex (CCVC: 0.361°N, 78. 349°W), one of
36 the largest volcanic centres in the northern part of the Ecuadorian Andes, is located
37 ~50 km north of Quito. Its southern flanks are covered by pyroclastic deposits related
38 to the Cuicocha caldera-forming eruption, which is one of the most explosive events
39 to have occurred in the Ecuadorian volcanic arc during the Holocene (von
40 Hillebrandt, 1989; Hall and Mothes, 1994; Pidgen, 2014). Highly populated (approx.
41 thirteen thousand inhabitants - [https://www.ecuadorencifras.gob.ec/base-de-datos-](https://www.ecuadorencifras.gob.ec/base-de-datos-censo-de-poblacion-y-vivienda/)
42 [censo-de-poblacion-y-vivienda/](https://www.ecuadorencifras.gob.ec/base-de-datos-censo-de-poblacion-y-vivienda/)) towns like Cotacachi, Quiroga, and Imantag have
43 developed on top of these deposits without considering the hazards related to living
44 close to a potentially active volcano.

45 Over the last decades, large explosive eruptions have occurred worldwide (e.g.,
46 Chaitén 2008, Lara et al., 2009; El Reventador 2002, Hall et al., 2004; Mt. Pinatubo
47 1991, Newhall and Punongbayan, 1996; among others) highlighting the importance
48 of understanding the eruptive chronology of poorly known volcanic centres or
49 complexes such as Cotacachi-Cuicocha; especially if they have displayed highly
50 explosive activity in the past and are in close proximity to a large population.

51 During the past thirty years, the IG-EPN (Instituto Geofísico, Escuela Politécnica
52 Nacional, Ecuador) and the IRD (Institut de Recherche pour le Développement,
53 France) have conducted several studies intended to reconstruct the eruptive
54 chronology of the main Ecuadorian volcanic centres, such as Chachimbiro (Bernard
55 et al., 2014), Cayambe (Samaniego et al., 1998; Samaniego et al., 2005), Imbabura
56 (Le Pennec et al., 2011; Andrade et al., 2019), Cotopaxi (Hall and Mothes, 2008),
57 Antisana (Hall et al., 2017), Pichincha (Robin et al., 2010), Pululahua (Andrade et
58 al., 2021; Vásconez Müller et al., 2022), Atacazo-Ninahuilca (Hidalgo et al., 2008),
59 Tungurahua (Hall et al., 1999; Bablon et al., 2018), Chimborazo (Samaniego et al.,
60 2012), Carihuairazo (Samaniego et al., 2022), Sangay (Monzier et al., 1999,
61 Valverde et al., 2021), and others along the Ecuadorian Volcanic Arc (Bablon et al.,
62 2020). These studies aim a better understanding of the development of the
63 Ecuadorian arc volcanoes and strongly contribute to volcanic hazards assessment.

64 This work is part of this long-term program and aim to fill a gap concerning the
65 Cotacachi-Cuicocha eruptive chronology.

66 Previous unpublished research has been mainly devoted to the Cuicocha caldera-
67 forming eruption products (von Hillebrandt, 1989; Pidgen, 2014), and more recently
68 to the current gas emissions observed in the caldera lake (Sierra et al., 2020; Melián
69 et al., 2021). Indeed, Cuicocha volcano seismic and degassing activity is closely
70 monitored by the Instituto Geofísico of the Escuela Politécnica Nacional University
71 (IG-EPN) from Ecuador (Sierra et al., 2020). However, despite its proximity to
72 densely populated areas, the eruptive history of the CCVC remains poorly
73 documented. The purpose of this work is to provide a first geological map of the
74 whole volcanic complex to address the lack of knowledge about the evolution of
75 CCVC, based on new chronological, petrographic, and chemical data collection.

76

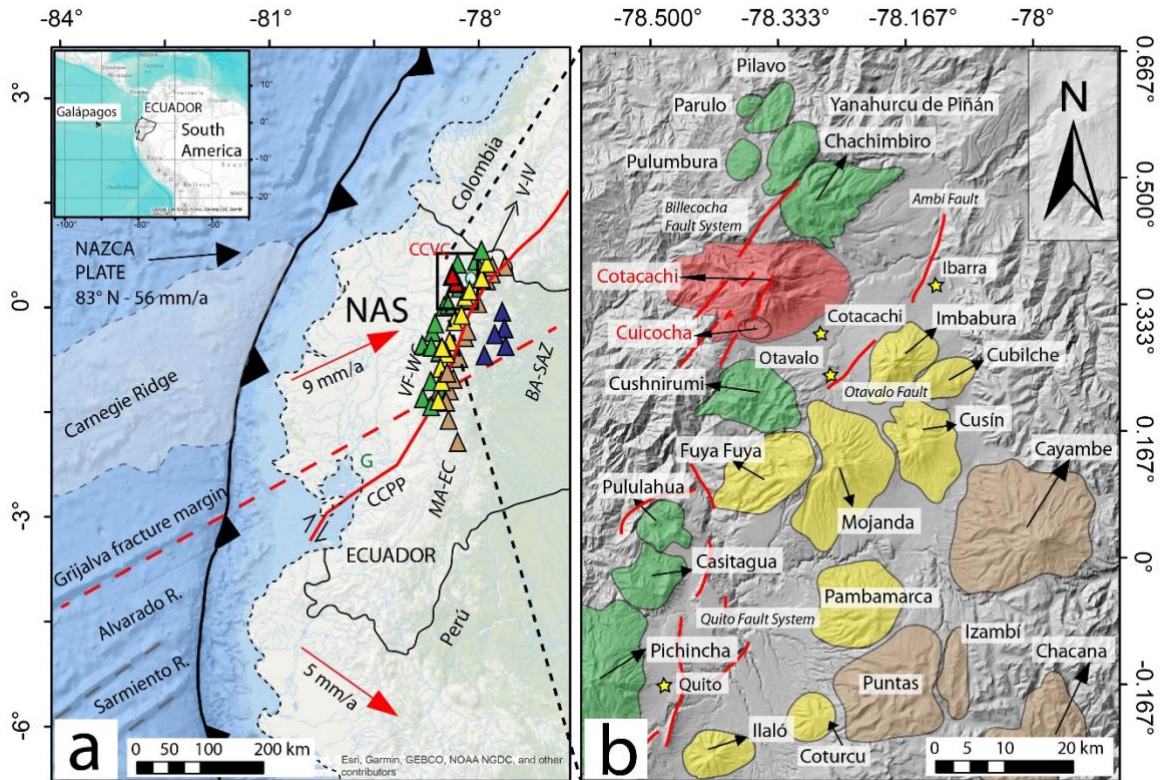
77 **2. GEOLOGICAL CONTEXT**

78 **2.1. Geodynamical and geological context**

79 The Ecuadorian volcanic arc results from the subduction of the oceanic Nazca plate
80 beneath the South American continental plate (Hall and Wood, 1985; Barberi et al.,
81 1988), with a convergence rate of 56 mm.yr^{-1} (relative to the stable Brazilian shield;
82 Trenkamp et al., 2002; Nocquet et al., 2014; Fig. 1). As a result, the Ecuadorian Arc
83 is divided into four north-south volcanic alignments, which are located along the main
84 morpho-structural domains (i.e., Western Cordillera, Inter-Andean Valley, Eastern
85 Cordillera, and the sub-Andean zone; Hall et al., 2008). The CCVC is constructed
86 on the Western Cordillera basement, a Late Cretaceous mafic volcanic complex
87 (Pallatanga and Río Cala units; Fig. 2) and related sedimentary rocks (Natividad
88 Unit; Fig. 2). These basement is interpreted as a part of the Caribbean-Colombian
89 Oceanic Plateau with overlapping deposits of an intra-oceanic magmatic arc
90 sequence, accreted to the continental margin during the Late Cretaceous (Goosens
91 and Rose, 1973; Feininger and Bristow, 1980; Hughes and Pilatasig, 2002; Kerr et
92 al., 2002; Jaillard et al., 2004; Pratt et al., 2005; Spikings et al., 2005; Luzieux et al.,
93 2006, Vallejo et al., 2006, Vallejo et al., 2009, Vallejo et al., 2019). These mafic
94 terrains also present quartz-diorite intrusions such as the Apuela batholith, dated at

95 16.5 ± 1.1 Ma (van Thournout, 1992; Boland et al., 2000. Fig. 2). Finally, the Late
 96 Oligocene – Early Miocene Silante formation (Vallejo et al., 2020) closes off the
 97 basement sequence below Cotacachi and consists of a succession of continental
 98 volcanoclastic sediments (Hughes and Bermudez, 1997; van Thournout, 1992;
 99 Boland et al., 2000).

100



101

102 *Figure 1. a) Geodynamic context of the Ecuadorian volcanic arc (modified from Yepes et al., 2016)*
 103 *and the spatial location of the four volcanic alignments (Bernard and Andrade, 2011; Hall et al., 2008).*
 104 *VF-WC: volcanic front of the Western Cordillera (green, red triangles for Cotacachi and Cuicocha*
 105 *volcanoes), V-IV: volcanoes of the Inter-Andean Valley (yellow), MA-EC: the main arc of the Eastern*
 106 *Cordillera (brown), and BA-SAZ: the rear arc of the Sub-Andean zone (blue). The main morpho-*
 107 *tectonic structures are NAS (North Andean Sliver), CCPP (fault system of Chingual-Cosanga-*
 108 *Pallatanga-Puná), and the Billecocha, Huayrapungo and Quito fault systems (Ego et al., 1996; Eguez*
 109 *et al., 2003; Jomard et al., 2021), and Río Ambi and Otavalo faults (Alvarado et al., 2016; Andrade*
 110 *et al., 2019); G: City of Guayaquil. b) Close-up view of the CCVC area, with the different volcanic*
 111 *systems colored as in a). Active faults from the Billecocha Fault System are shown with red lines, and*
 112 *cities are located with a yellow star.*

113

114 **2.2. Neotectonic context: the Billecocha Fault System (BFS)**

115 The Billecocha Fault System (BFS. Ego et al., 1996; Eguez et al., 2003; Jomard et
116 al., 2021; Figs. 1 and 2) appears as an eroded plateau-like morphology over the
117 moorlands north of Cotacachi volcano (Fig. 3a), close to Cristococha Lake (Fig. 2
118 and 3b). The present morphology of the moorlands is related to the last glaciation
119 (ca. 14 - 33 ka; Clapperton, 1990) and subsequent levelling out by the deposition of
120 volcanic deposits during the Holocene (Ego, 1996). The Billecocha Plateau and its
121 surrounding volcanoes are heavily affected by active faulting characterized by
122 straight, sharp, and discontinuous scarps (Jomard et al., 2021). These structures
123 possibly accommodate the convergence stresses of the Nazca plate subduction
124 beneath South America through the suture planes of the Cretaceous-Eocene
125 accretions (Boland et al., 2000; Hughes and Pilatasig, 2002). In this context, the BFS
126 could correspond to a surface expression of a tectonic reactivation of the Pujilí
127 Suture (Baize et al., 2020; Jomard et al., 2021). The slip rate of Billecocha was
128 constrained at around 2 mm/yr (Ego et al., 1996; Eguez et al., 2003). Despite being
129 located within the North Andean Sliver (NAS), the Billecocha Fault System has no
130 direct relation to neither the NAS stress regime nor to the Chingual-Cosanga-
131 Pallatanga-Puná (CCPP; Fig. 1) fault system (slip rate of 8-10 mm/yr; Nocquet et al.,
132 2014; Alvarado et al., 2016). The approximate length of the Billecocha fault system
133 is 6-7 km, striking approximately north 25° and dipping to the south-east (Eguez et
134 al., 2003). This structure has also been considered as a normal fault due to the
135 presence of scarps, sag-ponds, and drainage cuts (Ego et al., 1996; Eguez et al.,
136 2003). The morphology of the fault scarp and some detailed studies of kinematics
137 and chronology in the associated stratigraphy suggest that its last movement
138 occurred between 5.7 and 10 ka (Ego et al., 1996, Eguez et al., 2003). This
139 assumption was corroborated by Jomard et al. (2021), who mention that the current
140 activity of this fault system is low.

141

142 **3. ANALYTICAL METHODS**

143 Several field campaigns resulted in the detailed study of 79 outcrops (Appendix table
144 A and appendix figure A.1) related to the Cotacachi-Cuicocha Volcanic Complex.
145 Fieldwork included geological mapping (1:25.000 scale) and sampling of the

146 principal stratigraphic units, resulting in a collection of 52 unaltered samples for
147 geochronological, petrographic, and geochemical analyses.

148

149 **3.1. Geochronology**

150 Considering the volcano stratigraphy, as well as the sample freshness and their low
151 vesicularity, we selected 9 lava samples and one juvenile block from a block-and-
152 ash-flow deposit. These samples were dated using the potassium-argon (K-Ar)
153 method (Table. 1a) with the unspiked Cassinol-Gillot technique (Cassinol and
154 Gillot, 1982; Gillot et al., 2006), which was shown to be suitable for calc-alkaline
155 samples from Quaternary arc volcanoes (e.g., Germa et al., 2011; Ricci et al., 2015;
156 Bablon et al., 2018). This technique determines the radiogenic argon ($^{40}\text{Ar}^*$) content
157 of the sample and compares the $^{40}\text{Ar}/^{36}\text{Ar}$ ratios of both the sample and the
158 atmosphere measured in the same condition. Since the groundmass of a lava flow
159 is the last phase to crystallize when it cools after being erupted, its initial $^{40}\text{Ar}/^{36}\text{Ar}$
160 ratio corresponds to that of the atmosphere (*i.e.*, it does not contain any excess
161 $^{40}\text{Ar}^*$). On the contrary, phenocrysts such as plagioclase or biotite can carry inherited
162 ^{40}Ar that could significantly bias ages towards older values (e.g., Harford et al., 2002;
163 Samper et al., 2008). Therefore, we carried out our measurements on groundmass,
164 after removing phenocrysts using heavy liquids and magnetic separations. One
165 measurement was carried out on separated plagioclase crystals to compare the
166 result with the age obtained on groundmass. Details of analytical procedures, decay
167 constants, standards used, and uncertainty calculations are given in Bablon et al.
168 (2018). Both potassium and argon measurements were carried out at the GEOPS
169 laboratory at Orsay (Paris-Saclay University, France) using an Agilent 240 Series
170 AA flame absorption spectrometer and a multi-collector 180° sector mass
171 spectrometer, respectively. Measurements were performed at least twice to check
172 their reproducibility within their uncertainty range, at the 1σ level. Final ages and
173 uncertainties were calculated by averaging each analysis, weighted by their $^{40}\text{Ar}^*$
174 content.

175 The age of Cuicocha caldera explosive sequence was constrained by five new
176 radiocarbon ages obtained from charcoal and soil samples collected from pyroclastic

177 deposits. These samples were analysed at the Center for Isotope Research (CIO),
178 Groningen University (The Netherlands). Table 1b compiles the sample chronology
179 with conventional ^{14}C ages ($\pm 1\sigma$) as well as calibrated ages ($\pm 1\sigma$ and 2σ).
180 Conversion from conventional ^{14}C ages to standard and calendar ages was carried
181 out using the Calib 7.1 code (Stuiver and Reimer, 1993; Stuiver et al., 2005) and the
182 Northern Hemisphere calibration curve (IntCal20, Reimer et al., 2020).

183

184 **3.2. Petrography and geochemistry**

185 Thin sections of 52 samples were used to establish the samples petrography (modal
186 counting, texture, and structures) using a petrographic microscope (ZEISS AXIO
187 Scope A1; Appendix table B.1). Whole-rock chemical analyses of major and trace
188 elements for 61 samples spanning the entire volcanic history were carried out at the
189 Laboratoire Geo-Ocean (IUEM-UBO, Brest, France; Appendix table B.2).
190 Measurements were performed on agate-crushed powders by ICP-AES (Inductively
191 Coupled Plasma – Atomic Emission Spectroscopy). The relative standard deviation
192 is 1% for SiO_2 and 2% for the other major elements, except for low concentrations
193 ($<0.50\%$) for which the absolute standard deviation is 0.01%. The analytical
194 procedure is described in Cotten et al. (1995).

195

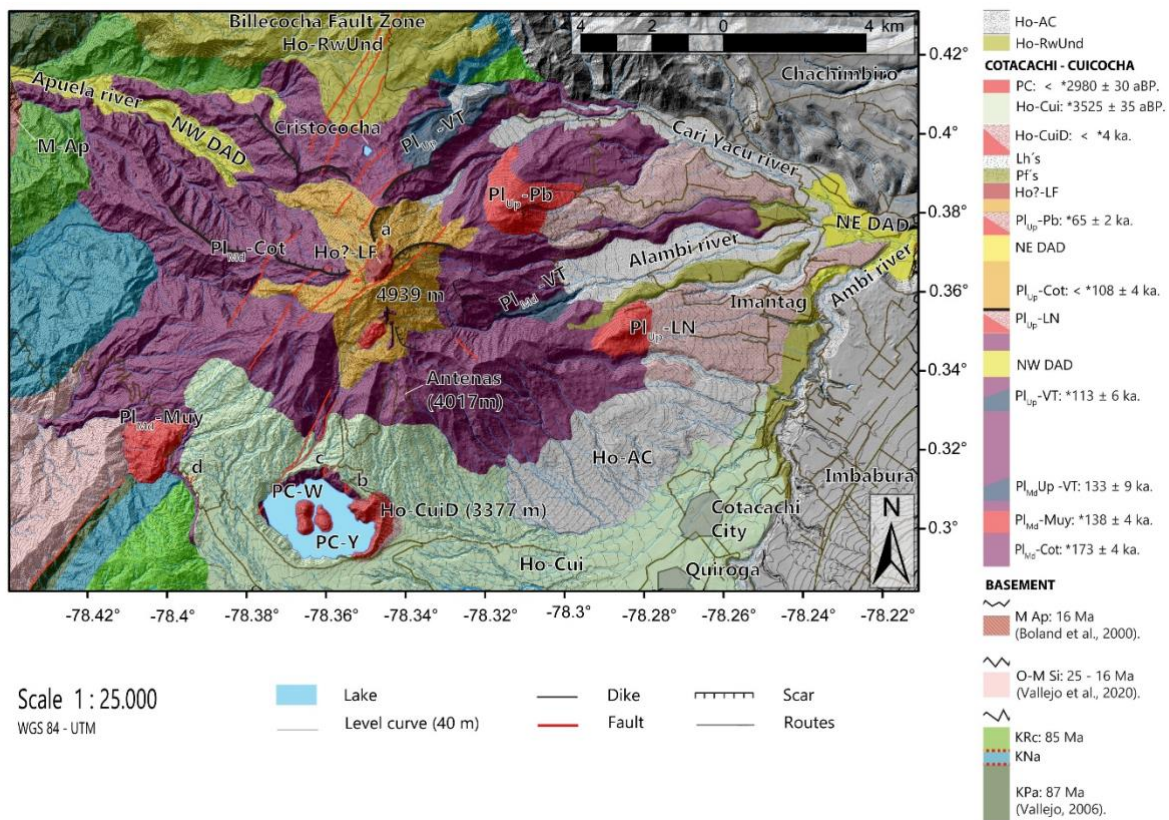
196 **3.3. Edifice volume, construction and erosion rates estimates.**

197 To quantify the morphological characteristics of this volcanic complex, we used two
198 digital elevation models (DEM), one developed by the Instituto Geográfico Militar
199 (IGM) of 30-m resolution, and a second model of 4-m resolution from SIGTIERRAS
200 project, by the Ministry of Agriculture and Livestock
201 (<https://www.agricultura.gob.ec/sigtierras/>). In this study, we used the 30-m for
202 regional (e.g., for traces of regional fault systems and description of the morphology
203 of stratigraphic units) and the 4-m one for local analyses (e.g., identification of small
204 volcanic structures as land-scarps, estimation of slopes and volume calculations).
205 Quantification of the minimum edifice volume, reconstruction, and erosion rate
206 estimates were performed in two different ways: The first method for volume

207 estimation considers linear interpolation using a MATLAB® script, which applies the
 208 volcano's baseline to create an interpolated grid that depicts the underlying
 209 basement (Table 2a). This method does neither consider those parts underneath the
 210 observed base nor those that were already eroded (see Andrade et al., 2021). In
 211 contrast, the second method, developed by Lahitte et al. (2012), and further
 212 improved by Germa et al. (2015), uses the ShapeVolc algorithm and ArcGis software
 213 to make numerical surface interpolations based on the present-day topography of
 214 the basement and the CCVC's crest elevations (Table 2b). It consists of numerical
 215 modelling of the pre-erosional shape of the volcano, based on the extrapolation of
 216 the uneroded surfaces such as crests (Dibacto et al., 2020).

217
 218
 219

4. RESULTS



220

221 *Figure 2. Geological map of the Cotacachi-Cuicocha volcanic complex. Ho-AC: Alluvial and colluvial*
 222 *deposits. Ho-RwUnd: Undifferentiated, reworked volcanoclastic deposits. PC: Post-caldera Domes*
 223 *(W: Wolf, Y: Yerovi). Ho-Cui: Cuicocha pyroclastic density currents. Ho-CuiD: Cuicocha pre-caldera*
 224 */ block and ash deposits. HO? -LF: Lava flows of the summit. Lh's: Lahar deposits of Cotacachi. Pf's:*
 225 *Pyroclastic deposits of Cotacachi. Summit lava flows. PI_{up}-Pb: Piribuela dome / block and ash*

226 *deposits. NE DAD: Northeastern debris avalanche deposit. PIUp-LN: Loma Negra dome / block and*
227 *ash deposits. PIUp-Cot: Upper Cotacachi Member. NW DAD: Northwestern debris avalanche deposit.*
228 *PIMd-Up-VT: Verde Tola Unit. PIMd-Muy: Muyurcu dome. PIMd-Cot: Basal Cotacachi Member.*
229 *MioAp: Apuela batholith. EOSi: Silante Unit. KRc: Río Cala Unit. KNa: Natividad Unit. KPa: Pallatanga*
230 *Unit. Letters: a, b, c and d are related to the locations of figure 5 outcrops of neotectonics. * For the*
231 *new ages obtained during this study.*

232

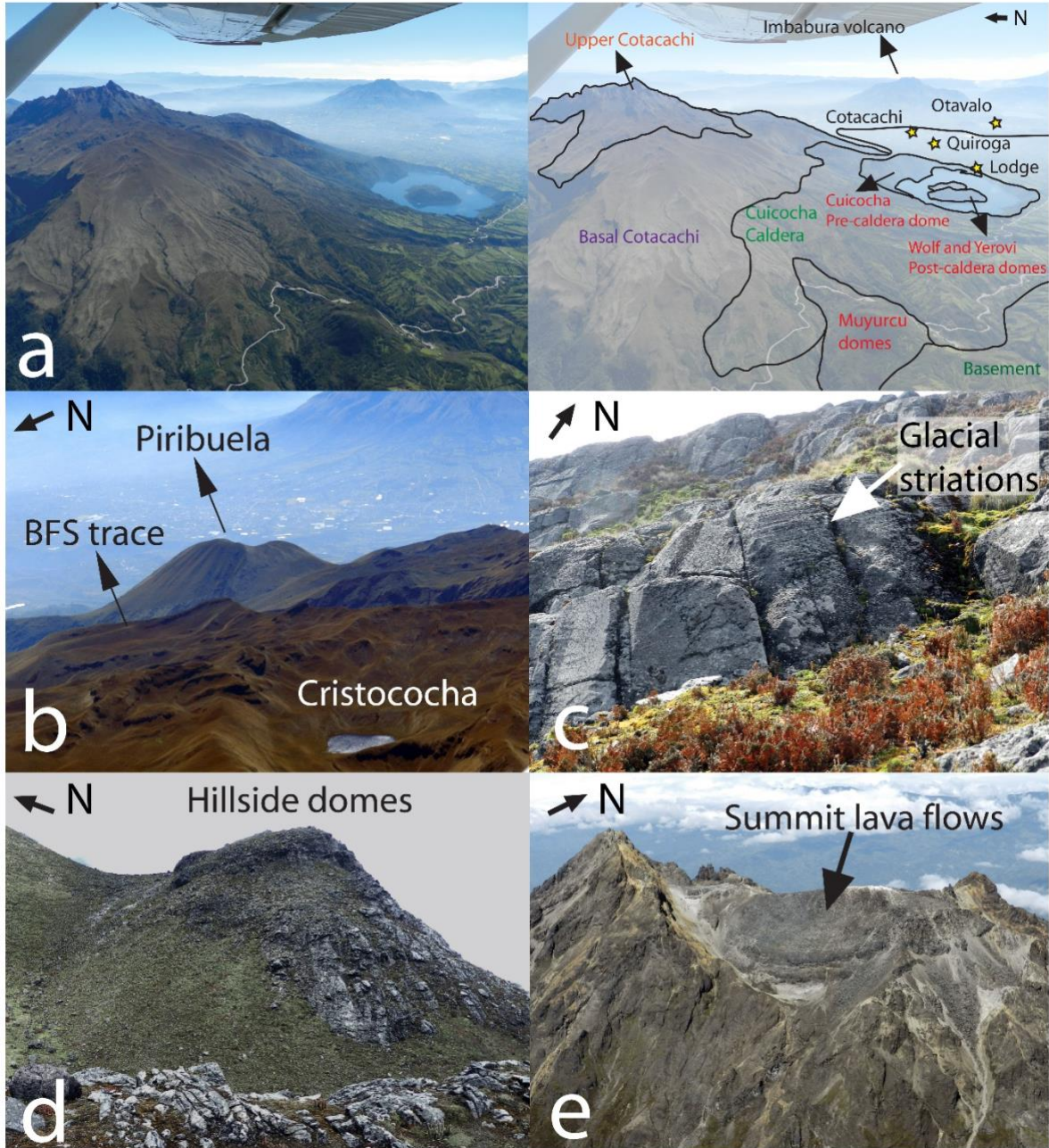
233 **4.1. Morphology and structure of CCVC**

234 The Cotacachi composite stratovolcano is the main edifice of the Cotacachi-
235 Cuicocha volcanic complex. Its basal surface covers an area of ~268 km², with a
236 north-south axis of 14-15 km and an east-west axis of 20-21 km (Figs. 2, 3).
237 Cotacachi volcano lower flanks are characterized by smooth slopes (6° - 25°;
238 Appendix figure A.2) and radial U-shaped glacial valleys, especially at the southern
239 and eastern flanks, which are partially filled with moraine deposits as well as local
240 and regional pyroclastic deposits. The moraines are in the high moorlands (between
241 3700 to 3800 m above sea level - asl) north of the edifice and are mostly visible
242 around a small glacial lake called Cristococha (3777 m asl; Fig. 3b). The presence
243 of radially oriented, deep glacial valleys, the frequent glacial striations displayed by
244 basal lavas (Fig. 3c), and the associated moraines, have been attributed to the Late
245 Pleistocene glaciations (Last Glacial Maximum - LGM), dated in the range of ca. 33
246 to 14 ka (Clapperton, 1990; Samaniego et al., 2012; Bablon et al., 2019) in this part
247 of the Andes. Towards the top of the edifice, the upper Cotacachi flanks (Fig. 3a) are
248 characterized by an abrupt change of slope (17° – 35°, Appendix figure A.2),
249 sculpting a pyramidal structure strongly affected by glacial erosion processes.
250 Indeed, the presence of smaller, young-looking moraines, reaching down to 3700 m
251 asl suggests that the terminal Cotacachi edifice was also affected by the glacial
252 advances younger than the LGM (i.e., the Younger Dryas and/or the Neoglacial
253 event, roughly dated at 10-12 ka and ~5 ka respectively; Clapperton, 1990). The
254 remnants of the last glaciers on the northern and eastern flanks of the volcano were
255 reported by Whymper (1892), Wolf (1892), and Troya (1913). Towards Cotacachi
256 volcano summit, on its southern flank, behind some relatively small hillside domes
257 (Fig. 3d), two major peaks (4939 m asl and 4756 m asl, respectively) aligned north-

258 south stand out. These peaks delimit a crater, inside which a dome-like structure
259 characterized by the absence of glacial erosion is observed (Fig. 3e).

260 Two groups of medium- to large-size scars of deep horse-shoe shaped depressions
261 are present on the north-western and north-eastern flanks of Cotacachi (3 to 10 km
262 wide; Appendix figure B). One is open towards the NW with a maximum width of 5-
263 6 km, while the second open towards the NE with an opening of 6-7 km. The lava
264 flows that constitute the main cone-building stage crop out at the inner walls of
265 escarpments. Additionally, younger, and smaller (2-3 km, Appendix figure B, black
266 coloured scars) scars were observed inside the largest one (Appendix figure B, blue
267 coloured scars) and may correspond to landslides produced by gravitational
268 processes or perhaps recent seismic activity (e.g., 7.0 – 7.3 M August 16th, 1868 -
269 Ibarra earthquake, Beauval et al., 2010; Madera, 1918).

270



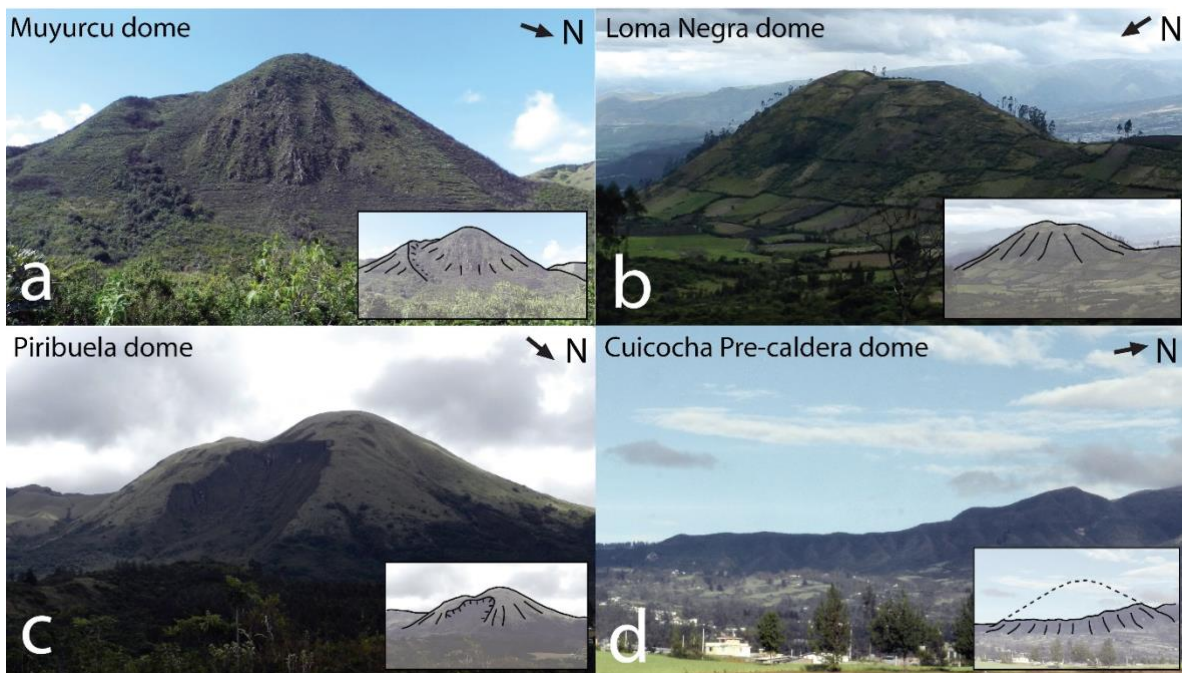
271

272 *Figure 3. a) Aerial photograph and illustration of the different stratigraphic members of the Cotacachi-*
 273 *Cuicocha volcanic complex. The yellow stars represent the populations closest to the volcanoes. b) Cristococha*
 274 *(0.396° N; 78.349° W) post-glacial lake and the different associated moraine deposits*
 275 *(between 3600 to 3900 m asl, on the north-western flanks of Cotacachi). c) Sub-horizontal glacial*
 276 *striated lava flows (0.350° N; 78.345° W) corresponding to basal Cotacachi (between 3450 to 4000 m*
 277 *asl, on the southern flank). d) Viscous lava flows (0.352° N; 78.346° W) forming a lava dome on the*
 278 *hillside southern flank of the volcano. e) Aerial photograph of the amphitheater of the Cotacachi*
 279 *volcano crater. Note the unglaciated summit lava flows (0.367° N; 78.346° W) or domes*
 280 *superimposed horizontally inside the crater.*

281

282 Moreover, several volcanic domes are distributed around the Basal Cotacachi edifice
 283 (Figs. 2, 4). Some of them are observed as compound domes (Muyurcu: 3502 m asl;
 284 Fig. 4a), and others as dome clusters (Loma Negra: 3066 m, Fig. 4b; Piribuela: 3871
 285 m asl, Fig. 4c). In addition, the remnants of the Cuicocha pre-caldera dome (3377 m
 286 asl; Fig. 4d) are observed west of Cuicocha caldera (Fig. 2), which has an elliptical
 287 shape and reaches 3.2 km from east to west and 2.3 km from north to south. The
 288 caldera rim is limited by steep walls (55 to 90°, 5.1 km²; Appendix figure A.2) which
 289 have been filled by almost 0.3 km³ of a meteoric water lake, occupying a minimum
 290 area of 3-4 km² (Gunkel and Beulker, 2009). The maximum water depth is 148 m,
 291 with a mean depth of 72 m (Gunkel and Beulker, 2009). Two east-west aligned islets
 292 located in the centre of the caldera lake correspond to post-caldera domes (Fig. 2).
 293 These islets are named Wolf (3247 m asl) and Yerovi (3142 m asl) and cover 0.5
 294 and 0.3 km² of the lake surface, respectively.

295



296

297 *Figure 4. Photographs of the peripheral domes of Cotacachi volcano (see Fig. 2 for geographic*
 298 *location). In chronological order: a) Muyurcu dome (0.323° N; 78.398° W), b) Loma Negra dome*
 299 *(0.351°N; 78.284° W), c) Piribuela dome (0.383° N; 78.314° W), and d) Cuicocha dome amphitheater*
 300 *(0.307° N; 78.348° W), observed from the east at the Selva Alegre – Quiroga road. Morphological*
 301 *features, as well as possible reconstruction of the Cuicocha dome and the scarp over the south-*
 302 *eastern flank of the Piribuela dome are shown as inserts at the bottom right.*

303

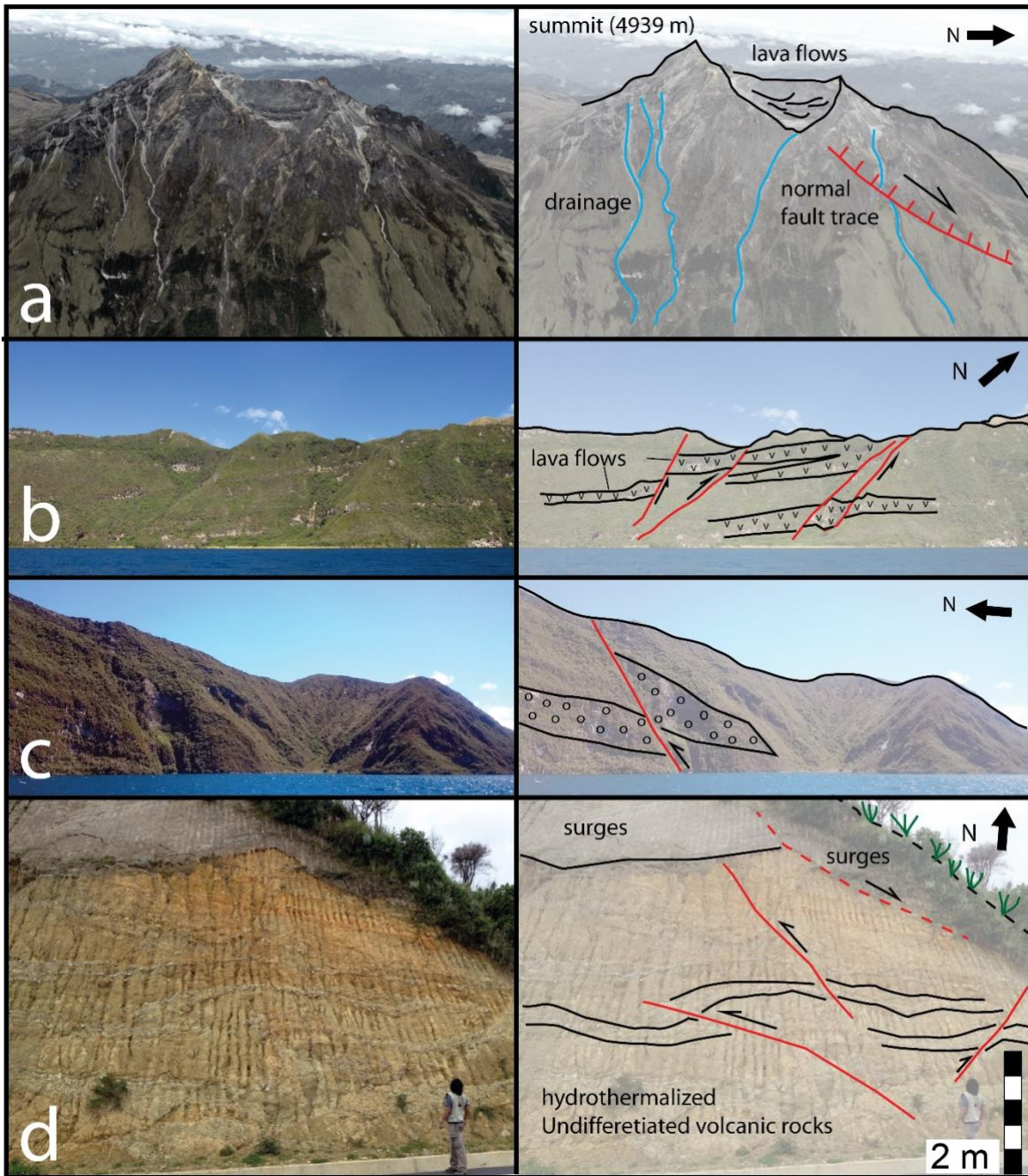
304

4.2. Main neo-tectonic structures of CCVC

305 Regional neo-tectonic structures of the Northern Andes cut across Cotacachi
306 composite volcano (Fig. 5a). Lineaments along with rupture zones crop out at the
307 western and northern walls of the Cuicocha caldera (Fig. 5b, 5c), extending across
308 Cotacachi from the southwest to the northeast (N22°E, N45°E - dipping 30 to 35° N-
309 NE). Displacements show apparent gravitational/extensional movements of the
310 basal Cotacachi lavas. The lineaments and their associated fault kinematics were
311 observed as trans-tensional/negative flower structure, and strike-slip faults with
312 secondary normal components (Ego, 1996, Eguez et al., 2003, this study). Finally,
313 the trace of the surface morphology looks like a horsetail structure (Fig. 2, Appendix
314 figure B).

315 Outcrops along the Cuicocha – Apuela road, exhibit small faults with positive flower
316 structures (Fig. 5d) with mostly compressive kinematics accompanied by some
317 secondary gravitational structures, whose azimuth strikes similar to the NE – SW
318 main Andean trend (Trenkamp et al., 2002; Eguez et al., 2003; Bourgois, 2013;
319 Alvarado et al., 2016; Yepes et al., 2016). At this locality the faults propagate through
320 the surge succession of Cuicocha caldera, a basal hydrothermally altered rock
321 sequence, and the older Cotacachi lava flows.

322



323

324 *Figure 5. Photographs of the different fault outcrops in the CCVC. The photographs and diagrams in*
 325 *two dimensions are shown according to the potential size of the structure: a) prolongation of the*
 326 *Billecocha fault system over the eastern flank (0.365° N; 78.339° W) of Cotacachi volcano edifice.*
 327 *The structure is observed as a normal type of fault with western vergence. The lava flows of the*
 328 *summit are not affected. b) northwestern wall (0.311° N; 78.373° W) of Cuicocha caldera lake,*
 329 *different structures of negative flower type are observed. c) northern wall (0.311° N; 78.354° W) of*
 330 *Cuicocha caldera lake, a potentially inverse structure is observed. d) structures of positive flower type*
 331 *(0.311° N; 78.394° W) in the Holocene deposits of Cuicocha, at the base of the surges some hydro-*
 332 *thermally altered and undifferentiated volcaniclastic deposits are observed.*

333

334 **4.3. Chronology of the CCVC**

335 ***Cotacachi Basal member***

336 *Main basal lava flows (PI_{Ma}-Cot)*

337 Basal Cotacachi lava flows (purple unit in Fig. 2) are a monotonous, ~500 m-thick
338 succession of sub-horizontal lava flows (Appendices figures C.1 and C.2), that reach
339 up to 5-7 km from the summit. The most representative outcrops are located at the
340 north-eastern and the south-western flanks of the volcano, between 2700 and 3900
341 m asl, as well as at the inner northern walls of the Cuicocha caldera. This succession
342 rests discordantly on the Cretaceous-Paleogene volcanic basement, covering a
343 surface of 107 km². Well-compacted matrix-supported breccias (30 vol.% of
344 andesitic lithics) are interlayered between the lava flows. The lavas are porphyritic
345 basaltic andesites and andesites (54.7 – 61.8 wt.% SiO₂), with a mineral assemblage
346 comprising plagioclase (11 vol. %), clinopyroxene (5 vol. %), orthopyroxene (3 vol.
347 %), and olivine (2 vol. %) (e.g., COTA-08). K-Ar ages obtained from two samples
348 taken near the base of the Cotacachi basal lava flows yielded ages of 173 ± 4 and
349 163 ± 4 ka, respectively (COTA 54 and COTA-01, Table 1a and Appendix figure
350 C.1). Three additional lava samples corresponding to the top of the basal lava flows
351 yielded ages of 110 ± 6, 108 ± 6 and 108 ± 4 ka, respectively (COTA-05, CUI-28,
352 and CUI-30A samples, Table 1a, Appendix figure C.1).

353

354

355

356

357

358

359

360

361

Sample	Lab Code	Location	Longitude (m)	Latitude (m)	Member, Unit	Phase	K (%)	⁴⁰ Ar ⁺ (%)	⁴⁰ Ar ⁺ x 10 ¹¹ (at/g)	Age ± 1σ (ka)	Mean age (ka)	
a	COTA 54	17EQ86	Distal lava flow, SW flank	787198	10037876	Basal Cotacachi	Groundmass	1.510	4.72	2.6912	171 ± 4	173 ± 4
									6.07	2.7518	174 ± 4	
	COTA 01		Lava flow, E valley	798773	9838736	Basal Cotacachi	Groundmass	1.075	4.32	1.7989	160 ± 4	163 ± 4
									4.38	1.8683	166 ± 4	
	COTA 56	17EQ88	Muyurcu dome, SW flank	789687	10035549	Muyurcu dome	Groundmass	1.378	3.60	2.0004	139 ± 4	138 ± 4
									4.53	1.9669	137 ± 4	
	COTA 02		Lava flow, SE flank	800141	9839050	Verde Tola Unit	Groundmass	0.952	1.53	1.3566	136 ± 9	133 ± 9
									1.56	1.2926	130 ± 9	
	COTA 012		Proximal lava flow, S flank	795416	10038627	Upper Cotacachi	Groundmass	2.001	5.33	2.5751	123 ± 3	122 ± 8
									6.41	2.3856	114 ± 2	
									5.68	2.7248	130 ± 3	
	COTA 60	17EQ93	Distal lava flow, NE flank	797793	10045132	Verde Tola Unit	Groundmass	1.133	1.77	1.4370	121 ± 7	113 ± 6
									2.23	1.2733	108 ± 5	
	COTA 05		Lava flow, E flank	798715	9838058	Basal Cotacachi	Groundmass	1.175	2.12	1.3089	111 ± 5	110 ± 6
									2.13	1.3826	113 ± 6	
	CUI 28		Lava flow, S flank	796267	9836562	Basal Cotacachi	Groundmass	1.156	1.85	1.3150	107 ± 6	108 ± 6
								1.66	1.2859	107 ± 7		
CUI 30A		Lava flow, S flank	795354	9836039	Basal Cotacachi	Groundmass	1.522	2.40	1.3150	109 ± 5	108 ± 4	
								2.68	1.7491	110 ± 4		
								3.28	1.6799	106 ± 4		
								0.66	0.3353	173 ± 26		
COTA 26		Block from a PF deposit, NE flank	801184	10041881	Piribuela Dome	Groundmass	2.529	0.97	0.4492	231 ± 24	207 ± 25	
								3.88	1.7183	65 ± 2		
COTA 57	17EQ89	Lava flow, Cuicocha dome	795129	10032404	Cuicocha	Groundmass	1.302	6.08	1.6972	64 ± 1	65 ± 2	
								< 0.1	-0.0092	< 4		

362

363

Sample	Lab code	Locality	Longitude (m)	Latitude (m)	Unit	Type of sample	¹⁴ C age (years BP)	d ¹³ C (‰)	Calendar age range (2 sigma) - InCAL20 (cal BP)	Relative area (%)	Calendar age range (1 sigma) - InCAL20 (cal BP)	Relative area (%)
b	CUI-27C	GrA 54410	Organic soil under ash before surges	796378	10037549	Cuicocha	soil	5750 ± 35	-24.77	95	6449 - 6647	19
											6493 - 6565	50
	CUI-22A	GrA 54412	Soil under pyroclastic flow	790562	10034145	Cuicocha	soil	4470 ± 35	-23.01	95	4973 - 5290	4
											5041 - 5070	10
											5102 - 5135	12
											5167 - 5279	43
	CUI-27B	GrA 54408	Organic soil under surges	796378	10037549	Cuicocha	soil	3525 ± 35	-25.24	95	3895 - 3695	2
											3819 - 3849	19
	CUI-22B	GrA 54411	Pyroclastic flow and surges	790562	10034145	Cuicocha	charcoal	2980 ± 30	-26.00	92	3060 - 3249	46
											3301 - 3324	3
											3033 - 3040	1
	CUI-27A	GrA 54406	Soil under ash fall after Cuicocha	796378	10037549	Cuicocha	soil	2245 ± 30	-25.71	28	2295 - 2339	3
2152 - 2265											68	
											2160 - 2166	
											2177 - 2235	42
											2232 - 2301	23

364

365 Table 1. a) Potassium-argon (K-Ar) ages obtained in this study (see text for details). Column headings indicate sample
 366 name, lab code, outcrop location, member/unit, dated phase of the sample, potassium content in percent, radiogenic argon
 367 content in percent and in atoms per gram, age obtained for each measurement, weighted mean age in ka, given with 1-σ

368 uncertainty. Measurements were carried out on groundmass for all samples, and on plagioclase crystals for CUI 30A sample.
369 b) Radiocarbon ages obtained from charcoal and soil samples collected in pyroclastic deposits. ¹⁴C chronology table gives
370 the conventional ages ($\pm 1\sigma$), and the calibrated ages ($\pm 1\sigma$ and 2σ) to standard and calendar ages, using the Calib 7.1 code
371 (Stuiver and Reimer, 1993; Stuiver et al., 2005) and the Northern Hemisphere calibration curve (IntCal13, Reimer et al.,
372 2013; IntCal20, Reimer, 2020).

373 *Muyurcu domes unit (Pl_{Md}-Muy)*

374 Muyurcu (3502 m asl) (Fig. 4a) is a small (1.5 - 2 km in diameter, with a surface of
375 2.4 km²) compound dome, which is located at the lower south-western flank of
376 Cotacachi (red unit in Fig. 2). Muyurcu dome is composed of a porphyritic, light grey-
377 coloured andesite (60.2 – 61.7 wt.% SiO₂) with plagioclase (13 vol. %), pyroxene (8
378 vol. %), and rare amphibole phenocrysts (4 vol. %). A K-Ar age obtained from a lava
379 sample from the summit (Loma de la Virgen) yielded an age of 138 ± 4 ka (COTA-
380 56; Table 1a). Importantly, this age agrees with the stratigraphic position of this unit,
381 which is almost contemporaneous with the main lava flow succession of Cotacachi
382 volcano basal member.

383

384 *Verde Tola unit (Pl_{Up}-VT & Pl_{Md}-VT)*

385 The olivine-rich Verde Tola lava flow succession (dark blue unit in Fig. 2), that forms
386 the Verde Tola hill at the lower north-eastern flank of Cotacachi, reaches between
387 3400 and 3900 m asl. This unit comprises a <100 m-thick lava flow succession, with
388 individual lava flows having a maximum runout of 2-3 km from the inferred emission
389 centre. Another < 30 m-thick lava flow succession crops out at the south-eastern
390 flank of the volcano, by the headwaters (3300 m asl) of the Alambi river valley (Fig.
391 2), where they concordantly overlay the Cotacachi basal lava flows, and reach 3 km
392 from the emission centre at the highest point of the Verde Tola hill. These lavas are
393 porphyritic, olivine-bearing basaltic andesites (54.7 - 55.9 wt.% SiO₂), with a mineral
394 assemblage of plagioclase (9 vol. %), clinopyroxene (3 vol. %), orthopyroxene (3 vol.
395 %), and olivine phenocrysts (4 vol. %). Two lava samples of the Verde Tola unit from
396 the SE and NE flanks were dated at 133 ± 9 (COTA-02) and 113 ± 6 ka (COTA-60,
397 Table 1a, Appendix figure C.1), respectively.

398

399 *Loma Negra dome unit (Pl_{Up}-LN)*

400 Loma Negra (3066 m asl) (red unit in Fig. 2, Fig. 4b) is an eroded lava dome located
401 at the eastern flank of Cotacachi volcano, with a basal surface of 1.9 km². It is
402 covered by a thick layer of reworked, well-compacted, black-coloured soil displaying
403 angular andesitic lithics. Loma Negra is composed of a porphyritic, light grey-

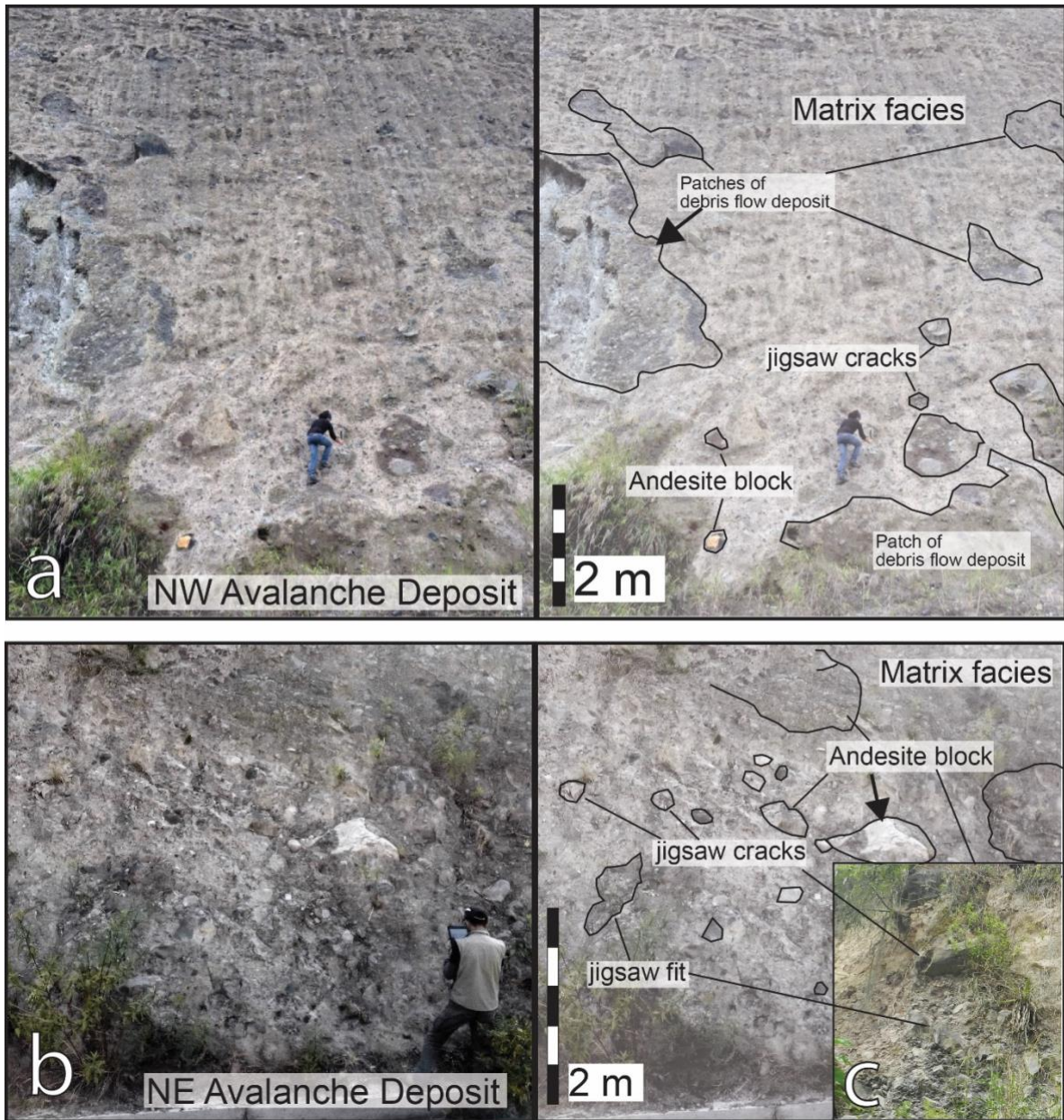
404 coloured andesite with plagioclase, amphibole, and scarce pyroxene phenocrysts.
405 In addition, a matrix-supported mono-lithological breccia that includes the
406 amphibole-bearing andesites (~20-30 vol.% of lithics) was identified at the eastern
407 flank of Loma Negra dome (red hatched area in Fig. 2). This deposit has an
408 estimated thickness of 10-20 m, reached 4-7 km from its inferred source, and covers
409 a surface of 10-12 km². Given its stratigraphic position cutting the Cotacachi lavas
410 on the SE flank, this dome appears to be younger than the lava flows of the
411 southeastern flank of Cotacachi, which were dated at ~110 ka.

412

413 *Northwestern debris-avalanche deposit (NW DAD)*

414 This unit crops out 40 km along the Apuela river inside the Intag valley (yellow unit
415 in Fig. 2), to the northwest and the southwest of the volcano. In the Intag valley, this
416 deposit overlies part of the Western Cordillera basement formed by the Apuela
417 quartz-diorite batholith (Boland et al., 2000). The NW-DAD has a maximum
418 thickness of 60-70 m from the bottom of the river valley (COTA 40; at 35 km from
419 the inferred source at north-western flanks of Cotacachi volcano, Appendix figure B)
420 and forms conspicuous and isolated terraces along the valley (Fig. 6a, Appendix
421 figure B). This deposit is a volcanic breccia characterized by blocky facies (approx.
422 30 vol.% of the deposit, e.g., individual lithics of basaltic andesites, andesites, and
423 some red and black volcanic scoria, as well as different patches of debris flow
424 deposits) with variable diameters from 0.5 to 1 m (4 m for the debris flow deposit
425 patches), embedded in a fine light-grey well-compacted matrix. The mineralogy of
426 andesite lithics found within this deposit is characterized by the ubiquitous presence
427 of pyroxene. Interestingly, no amphibole-bearing andesites were identified in the NW
428 DAD. Dense volcanic blocks display frequent jigsaw fractures. Mixed facies are also
429 present and constitute the main percentage (60 vol.%) of the distal avalanche
430 deposit. The deposit displays fine matrix injections and other small subrounded
431 lithics incorporated from the Western Cordillera basement, in addition to a small
432 number of lithics from the Apuela quartz-diorite batholith (less than 10 vol.%, ~0.25
433 m in diameter).

434



436

437 *Figure 6. Photographs of the (a) northwestern (Cota 40: 0.238046 N; 78.603827° W) and*
 438 *northeastern (Cota 17: 0.398295° N; 78.135906° W) debris-avalanche deposits of the Cotacachi*
 439 *volcano. The northwestern deposit is located at the road that leads to the Intag valley, close to the*
 440 *Apuela town. The northeastern deposit is located at the Ambi river valley, close to the Imantag town.*
 441 *An interpretation of the deposits and their main structures is shown to the right. (c) First plane picture*
 442 *of the jigsaw – cracks and fit inside the NE avalanche deposit.*

443

444 ***Cotacachi Upper member***

445 *Upper lava flows (Pl_{Up}-Cot)*

446 The upper member of the Cotacachi edifice (orange unit in Fig. 2) comprises a steep
447 succession of lava flows (Figs. 3a and e). Access to these highly altered outcrops is
448 very difficult, allowing only limited sampling of the southern flanks over 4000 m asl,
449 on the ascent route to the summit. This lava flow succession reaches between 250
450 and 350 m thickness with a 1-2 km runout from the summit. This unit covers a surface
451 of 16 km² and includes some interlayered volcanic breccias. Also, the lava flows form
452 an angular unconformity over the basal lava flow succession (Pl_{Mid}-Cot). This unit is
453 mainly formed by porphyritic andesites (59.8 – 60.7 wt.% SiO₂), which include some
454 andesitic enclaves. Some smaller (0.4 – 0.5 km²) viscous lava flows on the hillside
455 (Fig. 3d) and summit (HO - LF; Fig. 3e) are part of this volcanic unit and are formed
456 by siliceous andesites (61.9 – 62.3 wt.% SiO₂) with a mineral assemblage of
457 plagioclase (14 vol. %), orthopyroxene (2 vol. %), clinopyroxene (4 vol. %), and some
458 scarce amphibole (2 vol. %) and olivine phenocrysts (< 1 vol. %). Sample COTA12
459 taken from this unit yields an age of 122 ± 8 ka (Table 1a and Appendix figure C.1),
460 which, within uncertainties, overlaps with the ages obtained from the top of the lava
461 succession of Basal Cotacachi I (110 ± 6 to 108 ± 6 ka).

462

463 *Northeastern debris-avalanche deposit (NE-DAD)*

464 This unit crops out at 30 km from the Cotacachi volcano, forming the terraces of the
465 Cari-Yacu and Ambi rivers (yellow unit in Fig. 2, Fig. 6b), along the north-eastern
466 flank of the edifice. The NE-DAD appears beneath the Piribuela dome pyroclastic
467 deposits (Appendices figures C.2 and B) and has a maximum thickness of 15-20 m
468 (Cota 17, Cota 38). The NE-DAD is a consolidated volcanic breccia that includes
469 block-rich facies (~25 vol.% of the deposit), which comprise debris flow deposit
470 patches and large blocks of pyroxene-bearing andesites (typical of basal member),
471 as well as a few amphibolic andesites and dacites (typical of the upper member).
472 Some blocks (mainly andesites), from ~ 0.25 to 2 meters in diameter, showing
473 frequent jigsaw fractures are also observed. This deposit has a fine-grained and
474 cohesive matrix (75 vol.% of the deposit) and incorporated rounded basement lithics

475 (~ 0.5 m in diameter). The mineralogy and geochemistry of the lava blocks in this
476 avalanche deposit suggest that this event affected both basal and upper members
477 of the Cotacachi cone.

478 Given that lava samples from the overlying Piribuela domes (presented below) yield
479 an age of 65 ± 2 ka (Table 1a), and that the upper lava flows of the basal Cotacachi
480 yielded ages of 108 ± 6 and 108 ± 4 ka (Table 1a), we propose that this debris-
481 avalanche occurred between 108 ± 6 and 65 ± 2 ka. These ages agree with field
482 observations, that the NE-DAD is distributed across the Ambi river valley, which was
483 carved into the older Chachimbiro debris-avalanche deposit (dated between $405 \pm$
484 20 and 298 ± 32 ka; Bellver-Baca et al., 2019). In addition, long the right bank of
485 Ambi river, the NE-DAD is overlain by the Imbabura debris-avalanche deposit
486 (whose age is bracketed between 47 ± 6 and 30 ± 4 ka; Le Pennec et al., 2011;
487 Andrade et al., 2019; Appendix figure C.2).

488

489 *Piribuela dome (Pl_{Up}-Pb)*

490 Piribuela dome (3871 m asl, 3.6 km²) is located northeast of the Cotacachi summit
491 volcano (red unit in Fig. 2, Fig. 4c). It is composed of porphyritic light grey and red-
492 coloured dacites (63.6 – 64.8 wt.% SiO₂), which are the most differentiated eruptive
493 products found at the CCVC (Fig. 10a, b, c). The mineral assemblage of Piribuela is
494 composed of plagioclase (9 Avg. of Vol. %), amphibole (8 Avg. of Vol. %), biotite
495 (altered crystals substituted by Fe-Ti oxides), and scarce pyroxene phenocrysts (1
496 Avg. of Vol. %). At least two mono-lithological, matrix-supported breccias, with a high
497 percentage of dacitic lithics (~40 vol.%), were identified east-ward of the domes,
498 overlying the NE-DAD at the Imantag to Piribuela road (red hatched area in Fig. 2,
499 Appendix figure C.2), and interpreted as related to a young-looking scar present at
500 the south-eastern flank of the dome (Fig. 4c). These deposits have an estimated
501 thickness of 20-30 m, reaching 6-7 km from their inferred source, and covering a
502 surface of 7-8 km². A sample of a dacitic juvenile block from this deposit yielded an
503 age of 65 ± 2 ka (COTA26, Table 1a).

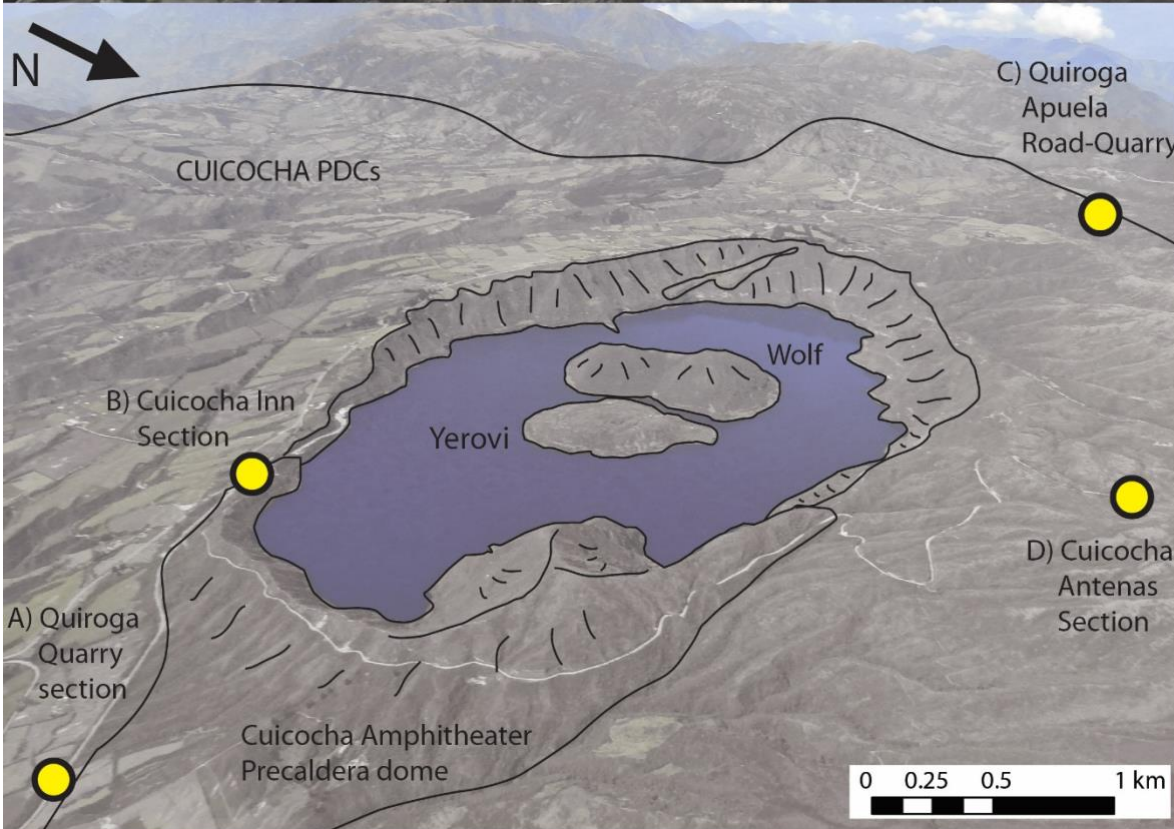
504

505 ***Cuicocha member***

506 *Pre-caldera unit (Ho-CuiD)*

507 The pre-caldera unit is composed of two sub-units, which correspond to the relicts
508 of the Cuicocha pre-caldera dome (red unit in Fig. 2, Fig. 4d), and some mono-
509 lithological volcanic breccias. Both are covered by a horizontal and compacted
510 deposit of orange-coloured fine-grained ash. This ash deposit shows a proximal
511 thickness of about 1 m decreasing to less than 5 cm at 16 km of distance.

512



515 *Figure 7. Aerial photograph of the Cuicocha caldera. The remnants of the pre-caldera dome are*
516 *observed, as well as the lake, the caldera rim, and the Wolf and Yerovi post-caldera domes. The*
517 *yellow circles represent the location of stratigraphic sections presented in figure 8 and sampling points*
518 *for radiocarbon ages (results are given in Table 1b).*

519

520 *Pre-caldera dome:* The most representative outcrops of the pre-caldera dome relicts
521 were identified in the caldera lake inner north-eastern walls and outside the caldera
522 (south-eastern flank) of Cuicocha, covering an estimated area of 1.7 km². Cuicocha
523 dome also constitutes the highest point in the caldera border (3377 m). Cuicocha
524 pre-caldera dome relicts display sub-vertical lava joints, which are light-grey
525 siliceous andesites (58.1 - 62.8 wt.% SiO₂), with a mineral assemblage of
526 plagioclase (14 vol. %) and amphibole (6 vol. %). Fe-Ti oxides are found replacing
527 almost entirely some amphibole phenocryst. Occasionally, a small percentage of
528 clinopyroxene (1 vol. %) is present in these rocks (Fig. 9). A sample of unaltered
529 lava from the dome yielded a poorly defined K-Ar age due to its very small radiogenic
530 argon (⁴⁰Ar*) content (< 0.1%, Table 1a), but indicates that the dome was emplaced
531 during Late Holocene times.

532 *Proximal monolithic breccia:* A relatively thin (1-2 m thick) layer of poorly sorted,
533 matrix-supported breccia with a high percentage of dacite lithics (40-50 vol.%) and
534 a dark-grey coloured, coarse-grained ash matrix covers the remnants of Cuicocha
535 pre-caldera dome. This deposit is visible on the dome's southern flank, along the
536 road that leads to the community of Apuela (1 km from the turn-off that leads to the
537 entrance to the Cuicocha caldera lake, Fig. 8b), and at the inner walls of the southern
538 caldera border.

539 At more distal outcrops (i.e., ~ 6 km westward along the same road), this matrix-
540 supported breccia is observed to have a reduced percentage of porphyritic dacitic
541 lithics (20-25 vol.%), as well as a dark grey to dark brown-coloured, medium-to-
542 coarse-grained reworked ash matrix (< 2 mm size).

543

544 *Syn-caldera deposits (Ho-Cui)*

545 The syn-caldera deposit succession is composed of two volcanoclastic subunits that
546 cover and smoothen the topography around Cuicocha lake (light green unit in Fig 2,

547 Fig. 8a). The syn-caldera deposit covers an area of $66.6 \pm 0.1 \text{ km}^2$ and reaches as
548 far as 13 - 15 km from the caldera lake towards the southeast (i.e., Hostería
549 Cuicocha entrance, Quiroga quarries, between 3000 to 2500 m asl, Fig. 8c), and 3 -
550 4 km to the northwest (i.e., road from Cuicocha lodge to Muyurcu dome, between
551 3000 to 3300 m asl). Other thinner deposits were found to the north over the
552 moorland (i.e., Las Antenas Road, between 3000 and 3900 m asl, Fig. 8d), reaching
553 3-4 km up the slope of the southern flank of Cotacachi.

554 The subunits are a basal and voluminous sequence of pumice-and-ash pyroclastic
555 density current deposits overlain by a less-voluminous layer of surge deposits.

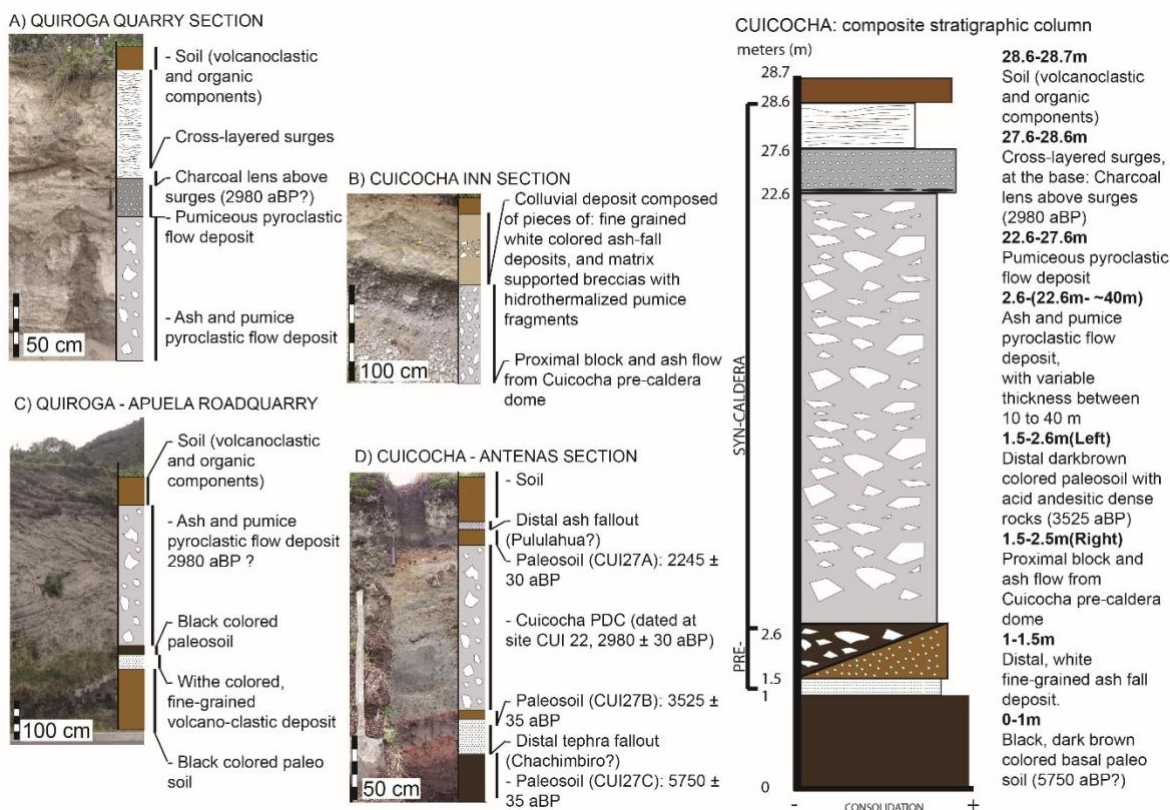
556 This syn-caldera pyroclastic succession overlays the pre-caldera units, and partially
557 covers the southern flanks of the Cotacachi basal member (Fig. 8).

558 *Pyroclastic density current (PDC) deposits:* This subunit is a 5 to 40 m-thick (average
559 of 20 m) succession of PDC deposits, formed by several pulses of caldera-forming
560 explosive activity. In the field, each pulse can be identified by its pink-coloured top,
561 which delimits PDCs horizons. At least 3 PDC layers are visible in the thickest
562 outcrops such as Quiroga quarry, located 7 km to the south-east from the caldera
563 lake. These deposits contain 30 vol. % of siliceous andesitic sub-angular pumice
564 lapilli and blocks (61.8 – 62.7 wt. % SiO_2), supported in a matrix of light grey-
565 coloured, medium-grained ash, which includes free plagioclase and hornblende
566 crystals. Similarly, the pumice mineral assemblage is plagioclase (9 Avg. of Vol. %),
567 amphibole (8 Avg. of Vol. %). In addition, dense lithics of Cuicocha pre-caldera dome
568 were found to make up at least 5 vol. % of these PCD deposits.

569 *Surge deposits:* Several pyroclastic surge deposits (i.e., dilute pyroclastic current
570 deposits) less than 1 m thick overlay the PDCs layers. They display a cross-bedded
571 stratification, are poorly sorted and fine-grained containing < 3 cm-size pumice lapilli
572 (and accretionary lapilli; Pidgen, 2014) and light-grey fine-grained ash. The juvenile
573 lapilli-pumice clasts have a siliceous andesitic composition (62.1 – 62.4 wt. % SiO_2).
574 Less than 3 vol. % of dense siliceous andesites from the pre-caldera dome
575 composed of plagioclase, amphibole, and scarce biotite were also incorporated.

576 Different centimetre thick reworked volcanoclastic layers are interspersed within this
577 succession between the pyroclastic flows and the pyroclastic surges, especially in

578 the moor area. Radiocarbon dating (Table 1b) of charcoal and soil samples found
 579 within Cuicocha syn-caldera deposits yields ages of 3525 ± 35 aBP (CUI-27B) at the
 580 base and 2980 ± 30 aBP (CUI-22B) at the top of the pyroclastic flows, which is
 581 concordant with the ages obtained by von Hillebrandt. (1989), of 2990 ± 300 a BP
 582 (Table. 1b).
 583



584
 585 *Figure 8. A B, C, and D are different stratigraphic sections of Cuicocha Caldera. To the right:*
 586 *Composite stratigraphic column of the section of the Cuicocha member. Note the stratigraphy*
 587 *section's location at figure 7. All the dates here presented belongs to this study, see table 1b.*

588
 589 *Post-caldera unit, Wolf and Yerovi domes (PC)*

590 This unit comprises four coalescent domes emplaced inside the Cuicocha caldera
 591 lake (Fig. 2, Appendix figure C.3), which form two volcanic islets called Wolf
 592 (maximum slopes of 48°) and Yerovi (maximum slopes of 35° , see section 4.1 for
 593 morphology and structure). The rocks that compose these domes are porphyritic
 594 siliceous andesites ($61.5 - 62.2$ wt.% SiO_2) bearing phenocryst of plagioclase (14
 595 Avg. of Vol. %), amphibole (12 Avg. of Vol. %), inside a glassy matrix. These domes

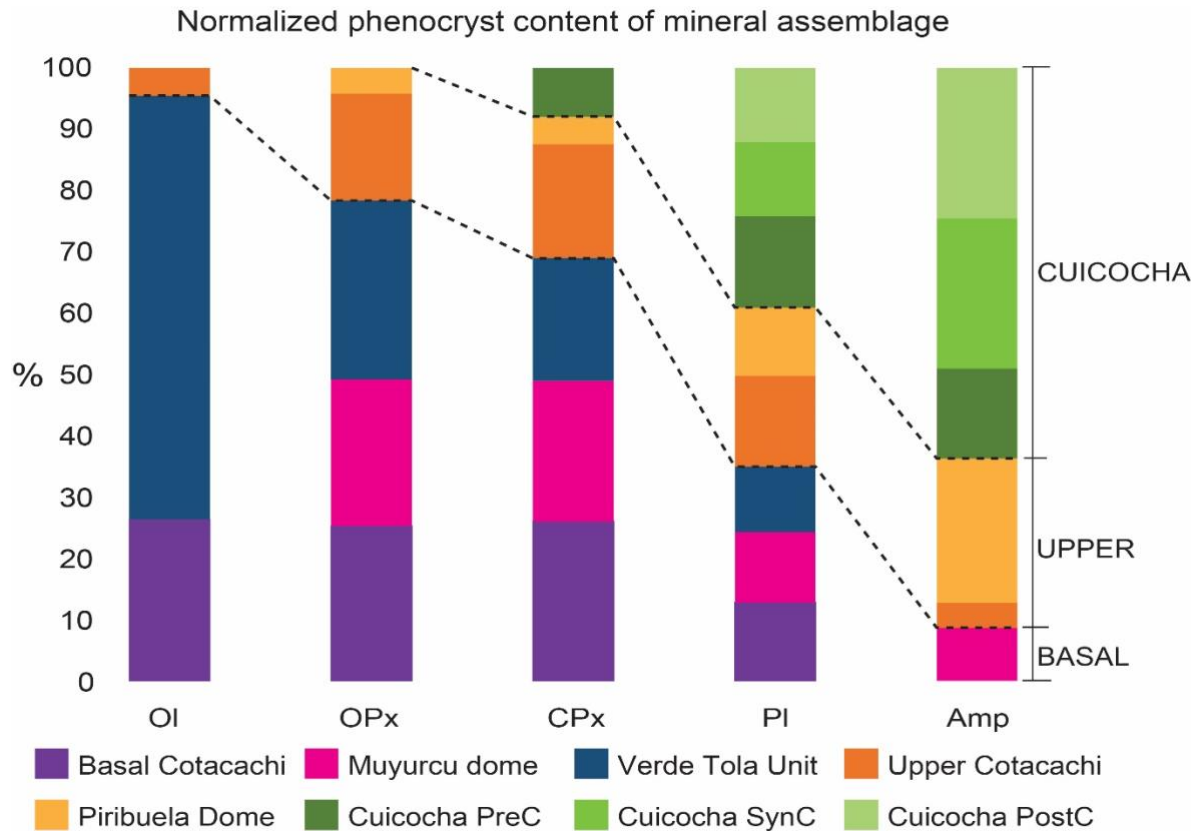
596 were emplaced after caldera formation, which means that they are younger or
597 coetaneous than 2980 ± 30 aBP (CUI-22B) (Table 1b).

598

599 **4.4. Main petrographic and geochemical characteristics**

600 The textures of the rocks that form the central edifice of Cotacachi are glomero-
601 porphyritic to ophitic, with mostly euhedral shaped phenocrysts, while the rocks that
602 form the domes and the products of Cuicocha Caldera are porphyritic with trachytic
603 texture. In both cases, the matrix is constituted by glass and microlites of plagioclase
604 ($< 100 \mu\text{m}$) and amphibole (for Cuicocha, Piribuela, and few in Muyurcu). Plagioclase
605 constitutes the dominant crystals, present in a similar percentage (11 – 12 vol. %) in
606 all stratigraphic members of the CCVC. On the contrary, the presence of olivine and
607 amphibole crystals is not homogeneous. The amount of olivine in the rocks of the
608 basal lava flows (2 vol. %) progressively decreases as the rocks become more silica-
609 rich (Upper member), to fully disappear at Piribuela dome and Cuicocha member
610 (Fig. 9, Appendix table B.1). The opposite is true for the amphibole phenocrysts,
611 which progressively appear in the upper Cotacachi lava successions (4 vol.%),
612 reaching a considerable content in the peripheral domes (Fig. 9), especially at
613 Cuicocha (8 vol.%).

614



615

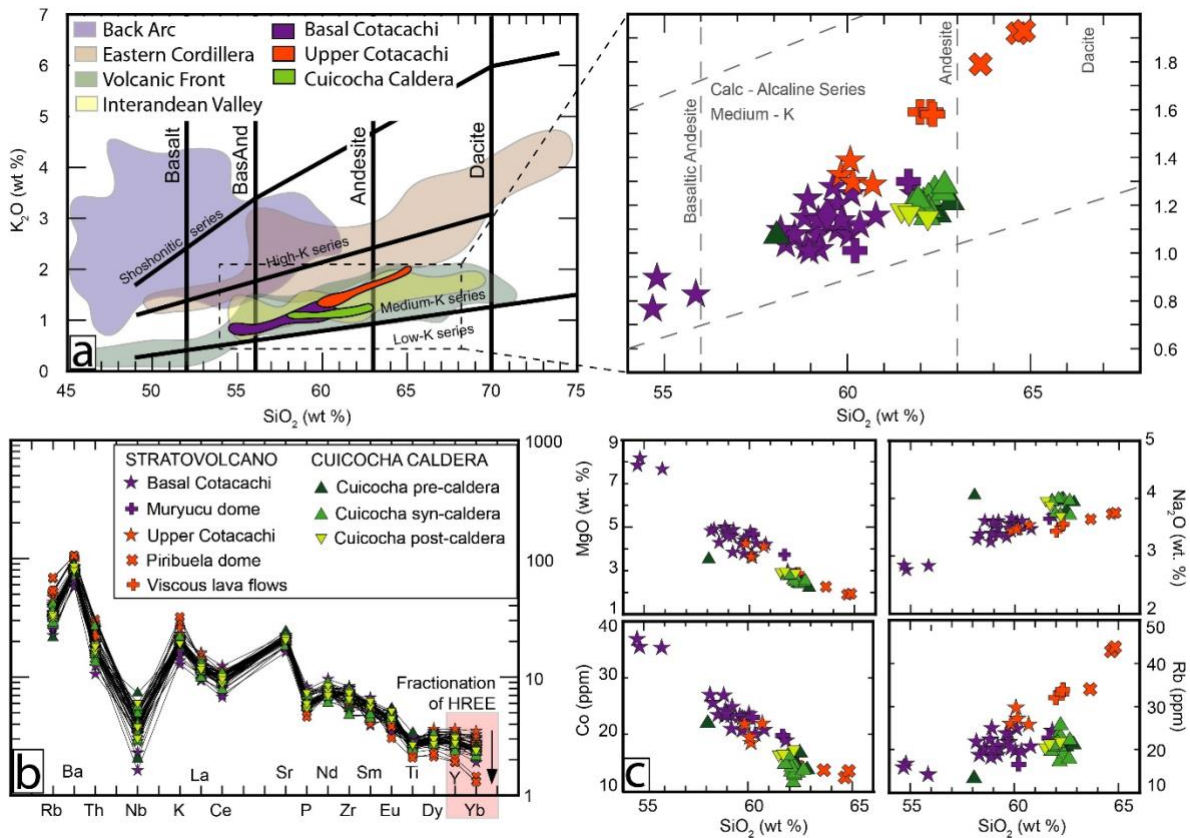
616 *Figure 9. Variability of Cotacachi - Cuicocha mineral assemblages in a base of a phenocryst*
 617 *normalization, see Appendix table B.1, note the transitional mineralogical change from Basal*
 618 *Cotacachi to Upper Cotacachi and Cuicocha member. Amp: amphibole, Pl: plagioclase, Cpx:*
 619 *clinopyroxene, Opx: orthopyroxene, Ol: olivine.*

620

621 CCVC rocks are calc-alkaline medium potassium basic to acidic andesites and
 622 dacites (54.68 – 64.83 wt.% SiO₂, 0.8 – 1.9 wt. % K₂O, Appendix table B.2)
 623 (Peccerillo and Taylor, 1976; Fig. 10a). They fall into the field of other erupted rocks
 624 produced in the Ecuadorian Western Cordillera (Hidalgo et al., 2012; Ancellin et al.,
 625 2017). In the primitive mantle normalized multi-elements diagram (Fig. 10b), all
 626 CCVC rocks display the Nb-negative anomaly and enrichments in Large Ion
 627 Lithophile Elements (LILE) as Rb, Ba, Th and K, typical of calc-alkaline rocks. A
 628 slight negative anomaly is also observed for P, while Heavy Rare Earth Elements
 629 (HREE) show mostly a flat pattern. Few samples from Cotacachi show a highly
 630 fractionated spectrum specially for Yb (Fig. 10b).

631 Major elements such as MgO, FeO, and CaO show negative correlations with silica,
 632 while Na₂O and K₂O show positive ones (Fig. 10c) as well as transition metals such

633 as Co, Ni, Cr, and Sc, show a compatible behaviour, illustrated by the Co vs. SiO₂
 634 diagram in figure 10c. In contrast, the Light Rare Earth Elements (LREE, e.g., Ce,
 635 La), and some Large Ion Lithophile Elements (LILE, e.g., Rb, Ba), show incompatible
 636 behaviour, illustrated by the Rb vs. SiO₂ diagram (Fig. 10c). Th, Rb, La, and Ba in
 637 Cuicocha rocks follow the same pattern as K₂O.
 638



639
 640 *Figure 10. a) Left: K₂O vs. SiO₂ diagram from Peccerillo and Taylor (1976) for representative samples*
 641 *of the Ecuadorian Volcanic Arc (modified from Hidalgo et al., 2012). The CCVC samples are*
 642 *highlighted. Right: Zoom to CCVC K₂O vs. SiO₂ members and units. b) Diagram of trace element*
 643 *content of CCVC rocks normalized to the primitive mantle (Sun and McDonough, 1989), note the high*
 644 *fractionation of the HREE (e.g., Yb) highlighted in the red-colored square. c) Representative Harker*
 645 *diagrams (MgO, Na₂O, Co and Rb) of CCVC members and units.*

646

647 **4.5. Bulk volumes and eruptive rates**

648 *Bulk volumes*

649 Results obtained using the interpolation MatLab script (see Andrade et al., 2021)
 650 with input surface values of $107 \pm 3 \text{ km}^2$ and heights ranging between 2519 and
 651 4939 m asl, yield an estimated minimum bulk volume of $56 \pm 4 \text{ km}^3$ for all CCVC
 652 proximal eruptive products currently remaining (i.e., the non-eroded volume; Fig. 11),
 653 where the $\pm 4 \text{ km}^3$ represent the standard deviation of the analytical results. However,
 654 to reduce the uncertainty of this method we must consider an error of $\pm 2\%$ in the
 655 cartographic boundary used by the script, which can modify the resulting volume by
 656 up to $\pm 10 - 20 \%$. Applying the ShapeVolc reconstruction method (Lahitte et al.
 657 2012), we calculated a minimum bulk volume of emitted material of $91 \pm 25 \text{ km}^3$ for
 658 the end of the CVCCs main construction stage (approx. 100 ka). The difference
 659 between the current ($56 \pm 4 \text{ km}^3$) and the reconstructed volume ($91 \pm 25 \text{ km}^3$) is 36
 660 $\pm 9 \text{ km}^3$, which represents the eroded volume since the end of the construction of
 661 the Upper Cotacachi, i.e., during the last 100 ka, which defines an erosion rate of
 662 $0.3 \pm 0.1 \text{ km}^3/\text{kyr}$ (Table 2b). We can assume a similar average erosion rate for both
 663 periods, since the syn-construction and post-construction periods (i.e., 173 ± 4 to
 664 $108 \pm 6 \text{ ka}$, and after $108 \pm 6 \text{ ka}$, respectively) both experienced a full glacial-
 665 interglacial cycle, and the average volume of the volcanic complex during these two
 666 stages is comparable. Therefore, applying the post-construction erosion rate of 0.3
 667 $\pm 0.1 \text{ km}^3/\text{kyr}$ to the syn-construction period of the basal and Upper Cotacachi
 668 members, the volume eroded between 173 ± 4 and $108 \pm 6 \text{ ka}$ is estimated at $21 \pm$
 669 6 km^3 . Finally, by adding this syn-construction eroded volume to that reached by the
 670 volcano at the end of its construction stage ($91 \pm 25 \text{ km}^3$), we obtain a total erupted
 671 volume of $112 \pm 31 \text{ km}^3$ for the uneroded Cotacachi basal and upper edifices (100ka
 672 stage, Fig. 11b).

673

a	Unit	Surface (km^2)	Extrapolated max. Volume (km^2)	Estimated minimum bulk Volume (km^3)	Estimated Volume (km^3)	Estimated Volume thick (m)	Estimated Volume thick (m)	Estimated average thick (m)	Maximum length (m)
	Basal Cotacachi	107.3			49 ± 4				
NW DAD	12	63		0.5 ± 0.2	1.1 ± 0.1	66	24	45	40
Muyurcu dome	2.4			0.3					
Loma Negra dome	1.9			0.1					

Upper Cotacachi	16.2			1.7					
NE DAD	12	41	0.2 ± 0.1	1.8 ± 0.5	20	16	18	30	
Piribuela dome	3.6			0.3					
Cuicocha pre-caldera	1.6			0.1					
Cuicocha syn-caldera	66.6			4.1					
Cuicocha post-caldera	0.8			0.04					
					Cuicocha total Volume (km ³)	56 ± 4	Cuicocha total volume (km ³)	4.2 ± 0.1	

674

b	Stage	Age max.	Age min.	Period	Raw volume	Eroded volume	Total, volume	Eruptive rate		Erosion rate	
		ka	ka	ka	km ³	km ³	km ³	km ³ /kyr	mm/yr	km ³ /kyr	mm/yr
	Construction Basal + Upper Cotacachi	173 ± 4	108 ± 6	65 ± 7	91 ± 25	21 ± 6	112 ± 31	1.7 ± 0.5	7.4 ± 2.2		
	Erosion since the end of Upper cotacachi construction	108 ± 6	0	108 ± 6			36 ± 9			0.3 ± 0.1	1.4 ± 0.4

675

676 *Table 2. a) Volume estimations in base of a MatLab interpolation using the 4m resolution digital*
677 *elevation model (Instituto Geográfico Militar - IGM). b) Result of volumes, eruptive and erosion rates*
678 *calculations obtained from ShapeVolc software (Lahitte et al., 2012) and given at 1-sigma accuracy.*

679

680 Due to the high erosion rate, the NW and NE debris-avalanche deposits are found
681 scattered in form of isolated terraces in the Intag and Ambi river valleys (Appendix
682 figure B), respectively. In addition, the traces of the supposed corresponding scars
683 in the higher flanks have been strongly eroded, impeding any avalanche volume
684 calculations based on the scar sizes (Appendix figure B). Therefore, minimum
685 volumes were calculated for the currently observed remaining debris-avalanche
686 deposit terraces, while maximum volumes were estimated by extrapolating the
687 potentially eroded deposit surface and using average thickness values of 45 and 18
688 m for the NW- and NE-DAD, respectively. In this manner, for the NW-DAD, which is
689 found between 3282 and 1960 m asl, we obtained volumes between 0.5 ± 0.2 km³
690 and 1.8 ± 0.5 km³, covering a surface of 12 to 41 km², respectively. For the NE-DAD,
691 found between 2315 to 1637 m asl, the estimated volumes range from 0.2 ± 0.1 km³
692 to 1.1 ± 0.1 km³, covering surfaces of 12 to 63 km², respectively.

693

694 For Cuicocha deposits, a current bulk volume of 4.2 ± 0.1 km³ was obtained using
695 the MatLab interpolation script including the pre-, syn- and post-caldera deposits,
696 which cover a surface of 68 km², with a variable altitude from 2535 to 3910 m asl.

697 This volume value agrees with the minimum volume of 4.1 km³ estimated by von
698 Hillebrandt (1989). In addition, tephra fallout deposits of Cuicocha cover a surface
699 of approximately 6.8 x 10² km², reaching the northern Ecuadorian coastline 176 km
700 away from the volcano. A volume estimation based on the Legros (2000) method for
701 a single isopach, results in 2 km³ of tephra fallout, using a representative thickness
702 of 0.08 m (calculation detailed in Vallejo Vargas, 2011).

703

704 *Eruptive rates*

705 A minimum bulk emission rate of 1.7 ± 0.5 km³/ka for the main basal Cotacachi lava
706 flows, was obtained using the step times of 65 ka (Cotacachi stratovolcano).

707 If we include the last age (2.98 ka) corresponding to the Cuicocha eruption (4.2 km³),
708 we obtain an emission rate of 0.068 ± 0.016 km³/ka (pause time of 62 ka, since the
709 formation of the Piribuela dome until the Cuicocha pre-caldera dome development),
710 corresponding to this last period of CCVC construction. Such drop in Cotacachi
711 volcano bulk emission rate from 1.7 ± 0.5 to 0.068 ± 0.016 km³/ka indicates a
712 progressive decrease in its eruptive activity.

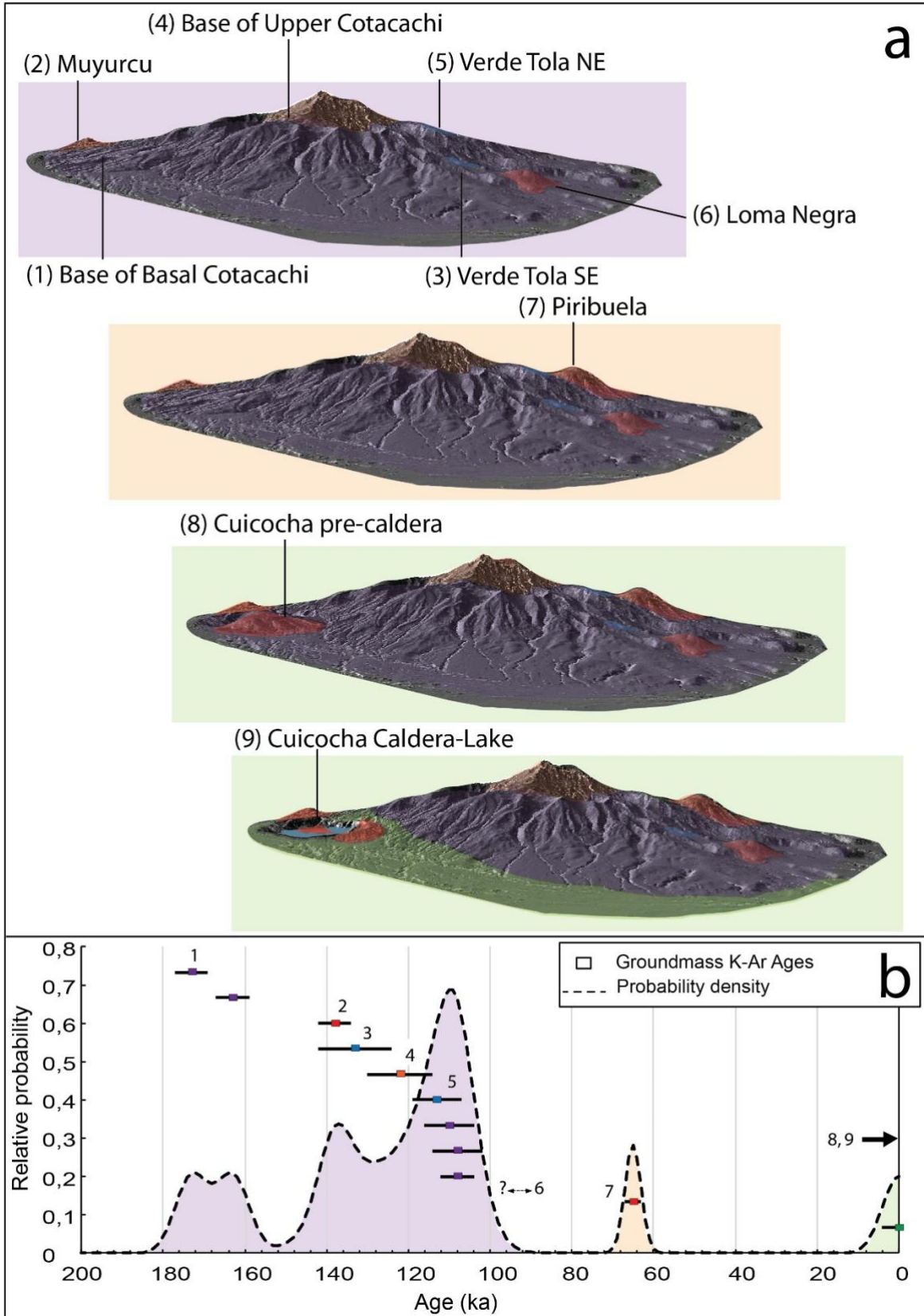
713

714 **5. DISCUSSION**

715 **5.1. Chronological evolution of CCVC**

716 According to the chronology obtained during this study, the eruptive activity of the
717 CCVC suggest this volcanic centre is among the youngest of the Western Cordillera
718 of the Ecuadorian Andes. Indeed, the Cotacachi stratovolcano (173 ± 4 to approx.
719 15 ka; this study, Fig. 11a) is younger than Cushnirumi (411 ± 8 to 383 ± 6 ka; Bablon
720 et al., 2020), Mojanda (1038 ± 87 to 194 ± 6 ka; Bablon et al., 2020) and Cusin (517
721 ± 8 to 495 ± 12 ka; Bablon et al., 2020). It is contemporary to the development of
722 Fuya Fuya (476 ± 38 to 28 ± 5 ka; Bablon et al., 2020), Chachimbiro (approx. 405 to
723 5 ka; Bernard et al., 2014, Bellver-Baca et al., 2019, Bablon et al., 2020), Cubilche
724 (45 ± 5 to 40 ± 5 ka; Navarrete et al., 2020, Bablon et al., 2020), and Imbabura (47
725 ± 6 to approx. 8 ka; Le Pennec et al., 2011, Andrade et al., 2019, Bablon et al.,
726 2020). Finally, the Cuicocha (3525 ± 35 aBP to 2980 ± 30 aBP) explosive volcanism
727 is one of the youngest in the northern part of the Ecuadorian Andes together with

728 Pululahua Dome Complex dated at approx. 2600-2300 aBP (Andrade et al, 2021;
729 Vásquez Müller et al., 2022).



731 *Figure 11. a) Morphological and chronological reconstruction of Cotacachi-Cuicocha Volcanic*
732 *Complex. b) Gaussian Age-probability spectrum (calculation detailed in Deino and Potts, 1992),*
733 *outlining potential gaps of activity between 100 and 65 ka, and between 65 and ~4 ka. Groundmass*
734 *K-Ar ages are shown with the same color used for units from figure 2.*
735

736 *Cotacachi strato-volcano*

737 The age probability curve (Fig. 11b) calculated from the K-Ar ages obtained here for
738 the volcanic complex shows six peaks of activity, with three growth gaps. It highlights
739 the formation of the basal stratovolcano (Cotacachi) between 180 and 100 ka. Within
740 this interval, the first short hiatus of activity is followed by the extrusion of the
741 southwest Muyurcu dome and the subsequent emission of lavas from the Verde Tola
742 unit (SE: 133 ka and NE: 113 ka). The younger construction phase of the Cotacachi
743 strato-volcano occurred between 122 and 108 ka. The following two stages of activity
744 (70 to 60 ka, and less than 10 ka, respectively) are associated with the extrusion of
745 the Piribuela (the most silica-rich dome of CCVC; dated at 65 ka) and Cuicocha
746 domes. Nevertheless, we must keep in mind that such age-probability curve is
747 biased by the low number of available ages, mostly due to the lack of sample from
748 difficult-to-access units (e.g., summit lava flows). Note that the plagioclase (CUI-30A)
749 age of 207 ± 25 ka is much older than the age obtained from the groundmass of the
750 same sample (Table 1a). This suggests that, as observed elsewhere (e.g., Singer et
751 al., 1998), plagioclase crystals could have been incorporated in the magma reservoir
752 and did not have time to be reset before the eruption. This led to an apparent K-Ar
753 age older than the age of the eruption. This example supports the importance of
754 carrying K-Ar ages on groundmass for young volcanic material.

755 The main cone-building stage (Middle to Upper Pleistocene, starting at 173 ± 4 ka)
756 of the Cotacachi cone is represented by the emission of a thick succession of
757 andesitic lava flows, which form the lower and middle flanks of the edifice,
758 constructed directly over the Cretaceous to Paleocene basement of the Western
759 Cordillera. Some peripheral domes were formed subsequently, starting with the
760 oldest south-western Muyurcu, at about 140 ka. Stratigraphic relationships show that
761 the south-eastern Loma Negra dome is younger than 108 ± 6 ka. During the period
762 between 140 and 108 ka, the lava flows of Verde Tola were emitted, the composition
763 (54.7 - 55.9 wt.% SiO₂) of which suggests an apparent effusive type of activity,

764 forming two isolated (SE: 133 ± 9 ka, NE: 113 ± 6 ka) olivine-bearing and
765 magnesium-rich basaltic-andesitic lava flow successions. A 5 km large amphitheatre
766 that opens to the NW cuts the basal lava flows of Cotacachi. The corresponding
767 debris avalanche deposits reach approx. 40 km along the Intag valley and are
768 characterized by the absence of amphibole-bearing andesites, which is typical for
769 the Upper Cotacachi member. Based on the description we suggest this first north-
770 western debris avalanche occurred before 108 ± 6 ka.

771 The upper and steep flanks of the Cotacachi stratocone represent the last phase of
772 development of the main cone-building stage (Cotacachi upper member). The
773 youngest ages of the Basal member (110 ± 6 and 108 ± 6 ka), overlap the oldest
774 age (122 ± 8 ka) of the Upper lava flow succession (Appendix figure C.1), which can
775 be interpreted as the loss of the youngest section of this building stage, due to the
776 intense erosion rate we have obtained here (0.3 ± 0.1 km³/kyr). The second partial
777 flank collapse event occurred on the north-eastern flank, leaving a debris avalanche
778 (NE-DAD) deposit that crops out towards the Ambi river valley and is covered by the
779 Piribuela deposits at the proximal facies and by the Imbabura DAD at its distal facies
780 (Appendix figure C.2). Interaction between the avalanche and the glacier has had an
781 important implication in the fluidization of the moving mass (Deline, 2009) of the NE-
782 DAD, giving the deposit an appearance of a big lahar. Since Piribuela dome was not
783 affected by the debris avalanche event and its associated deposits overlay the NE
784 avalanche, the NE-DAD must have taken place between 108 ± 6 and 65 ± 2 ka.
785 Following the discrimination between volcanic debris and rock avalanches (Dufresne
786 et al., 2021), we have tried to establish the origin of those observed at CCVC. Due
787 to the low juvenile clast content as well as the apparent structural control provided
788 by the Billecocha fault system, we propose that the debris avalanche events at
789 CCVC originated from tectonic disturbances rather than from violent eruptions. The
790 last evidence of eruptive activity of Cotacachi edifice corresponds to the summit lava
791 flows (Fig. 4e, Fig. 5a), which lack glacial erosion, suggesting an age younger than
792 the LGM (i.e., from 33 to 14 ka; Clapperton, 1990; Samaniego et al., 2012; Bablon
793 et al., 2019). In addition, Ego et al. (1996) suggests a specific period of activity for
794 the Billecocha fault system between 5.7 and 10 ka BP. Considering that the summit

795 lava flows have not been affected by the regional tectonics, Cotacachi activity could
796 have lasted until 15 - 10 ka BP. Cuicocha pre-caldera dome (^{14}C : 5750 ± 35 aBP to
797 3525 ± 35 aBP; Table. 2b), is the youngest volcanic dome in the evolution of the
798 CCVC, whose destruction resulted in the formation of the Cuicocha caldera lake.

799

800 *Cuicocha explosive event*

801 The caldera-forming eruption of Cuicocha is characterized by a large succession of
802 pyroclastic density currents (i.e., pumice and ash pyroclastic flows, and surges) that
803 covers a large surface (67 km^3 , Table 2a) around the caldera (von Hillebrandt, 1989;
804 Pidgen, 2014; Fig. 2, Fig. 7).

805 This explosive phase (Syn-caldera unit) is related to the destruction of the pre-
806 caldera Cuicocha dome and the formation of the first crater/depression. Successions
807 of poorly stratified pyroclastic-flow deposits are related to the paroxysmal phase of
808 the eruption (Pidgen, 2014). Additionally, the physical characteristics of Cuicocha
809 surge deposits (i.e., highly fragmented, fine-grained deposits, presence of
810 accretionary lapilli, and cross/layered stratification) reveal that an intense
811 phreatomagmatic activity took place during a new dome construction phase in a
812 subaqueous environment (i.e., inside the first caldera lake) (^{14}C : 2980 ± 30 aBP).

813 The Cuicocha eruption ended with the formation of the Wolf and Yerovi post-caldera
814 domes (von Hillebrandt, 1989; Pidgen, 2014). The volumes of $4.2 \pm 0.1 \text{ km}^3$ and ~ 2
815 km^3 obtained for the proximal PDC deposits and tephra fallout deposits, respectively,
816 classify this event with a Volcanic Explosivity Index of 5 (VEI= 5; Newhall and Self,
817 1982). Our data suggest that the pre-caldera lava dome formation, the syn-caldera
818 explosive phase, and the post-caldera dome growth of Cuicocha, occurred during a
819 period spanning roughly 1.5 ka, probably involving more than one eruptive event.

820 The resulting morphology produced by the above-described phenomena is a funnel-
821 shaped caldera, which main characteristic is their shape, resulting from the outward
822 widening of the vent, through erosive and gravitational mechanisms, such as
823 progressive subsidence of a highly fractured crater (Lipman, 2000; Cole et al., 2005).

824 Future work should address the formation of the observed Cuicocha depression in
825 more detail since the present interpretations are based on its morphology.

826

827 **5.2. Contextualizing volumes, erosion, and eruptive rates**

828 The erupted volume corresponds to the difference between the basement elevation
829 interpolation and the elevation model at the end of CCVC construction, while the
830 post-construction eroded volume corresponds to the difference between the
831 elevation model at the end of edifice construction and the present-day morphology.
832 As detailed in Bablon et al. (2018), eruptive rates were calculated using durations
833 derived from age differences between the beginning and the end of the main
834 construction stages, whereas post-activity erosion rate calculations involved the time
835 elapsed since the end of Cotacachi construction. Then, although both methods have
836 allowed estimating volumes, their limitation lies in the quantification of the cause-
837 effect produced by loss of data (Andrade et al., 2021; Vásconez Müller et al., 2022).
838 In this sense, estimated volume should be considered with caution and are
839 presented with a high uncertainty due to biases that can be induced by erosion (loss
840 of data from younger sequences), modelling of the basement elevation, as well as
841 the possible flank collapses.

842

843 By comparing the bulk volume results obtained for the current and the reconstructed
844 Cotacachi-Cuicocha Volcanic Complex (56 vs. 91 km³) with those of other andesitic
845 - dacitic volcanic complexes in the Ecuadorian arc (Pichincha volcanic complex: 30
846 to 250 km³, Robin et al., 2010; Chimborazo: 63 to 100 km³, Samaniego et al., 2012;
847 Imbabura: ~ 65 km³, Cushnirumi: ~53 km³, Bablon et al., 2020) and others with
848 similar characteristics in the Andes (Ampato Sabancaya – Peru: 44 - 54 km³,
849 Samaniego et al., 2016; El Misti – Peru: 70 km³, Thouret et al., 2001), we observe
850 that the CCVC is among the more voluminous volcanoes of the Northern and Central
851 Volcanic Zones of the Andes.

852 In contrast, the range of volumes obtained for the NW (0.5 – 1.8 km³) and NE (0.2 –
853 1.1 km³) avalanches are smaller than other Ecuadorian avalanche deposits (i.e.,
854 Sangay: ~33 km³, Valverde et al., 2021; Chimborazo: 10 – 12 km³, Samaniego et
855 al., 2012; Tungurahua: 8 km³, Hall et al., 1999; Cubilche: 3 km³, Roverato et al.,

2018), as well as others from continental volcanoes (i.e., Saint Helens-USA: 2.5 km³, Voight et al., 1981; Oshima – Japan: 2.5 km³, Satake and Kate, 2001).

Moreover, we estimated that 36 ± 9 km³ of material have been eroded since the end of Cotacachi construction (~100 ka), corresponding to an average erosion rate of 0.3 ± 0.1 km³/kyr. This erosion rate is one of the highest obtained in the Ecuadorian Andes, only comparable to those of Carihuairazo volcano (Samaniego et al., 2022), South Iliniza volcano (Santamaria et al., 2022) and the oldest stage of Tungurahua volcano (~0.2 ± 0.1 km³/kyr; Bablon et al. 2020). The high erosion rates in CCVC can be related to the combination of tectonic events with common erosion processes (such as glacial, fluvial and wind erosion) during its evolution.

Finally, the decrease observed for the CCVC's bulk emission rate, from 1.7 ± 0.5 for Cotacachi to 0.068 ± 0.016 km³/ka for Cuicocha, is similar to the case of Chimborazo volcano, which declines from 1.6 to 0.3 km³/ka, from the basal to the youngest cone, respectively (Samaniego et al., 2012).

871

872

873 **6. CONCLUSIONS**

874

The Cotacachi-Cuicocha Volcanic Complex (0.361° N; 78.349° W) is composed of a stratovolcano (Cotacachi: 173 ± 4 until the end of the Pleistocene), four peripheral/satellite domes (Muyurcu: 138 ± 4 ka; Loma Negra: younger than 108 ka; Piribuela: 65 ± 2 ka and Cuicocha pre-caldera: about 3 ka), and a funnel-shaped caldera, currently occupied by a lake, formed during a large explosive event dated at 2980 ± 30 a BP (4.2 ± 0.1 km³ of emitted material) that ended with the extrusion of two post-caldera domes. Cuicocha is considered a potentially active volcano that is currently monitored.

883

CCVC rocks ranges from basic to siliceous andesites and dacites (54.7 – 64.8 wt.% SiO₂), whose chemistry corresponds to medium potassium, calc-alkaline magmatic series and exhibits the typical trend of the rocks erupted at the Western Cordillera

887 and Inter-Andean Valley of the Ecuadorian Andes (Hidalgo, et al., 2012; Fig. 10).
888 Cuicocha siliceous-andesites are slightly depleted in K_2O and some trace elements
889 such as Th, Rb, La, and Ba, displaying a different trend to that of Cotacachi
890 stratovolcano and its peripheral domes. The mineral assemblage of the stratigraphic
891 members (Basal and Upper Cotacachi, and Cuicocha) of CCVC shows a
892 characteristic transition defined by the progressive disappearance of olivine and the
893 appearance of amphibole and biotite as silica content increases.

894

895 The CCVC, is one of the youngest (Middle Pleistocene to Holocene), and largest
896 (4939 m asl; 56 to 91 km^3 bulk volume) volcanoes in the northern Western Cordillera
897 of Ecuadorian Andes. Due to its height, its high elevation, and its proximity to active
898 faults, it has suffered a strong erosion ($\sim 0.3 km^3/kyr$), that should be linked to fluvial,
899 wind, glacial, and tectonic processes. This erosion rate is among the most important
900 of the entire Ecuadorian arc.

901

902 In addition, two small avalanches affected different volcano flanks (NW, along Intag
903 valley, and NE, along Ambi river valley flanks, respectively) at different stages of its
904 formation. The north-western avalanche (0.5 ± 0.2 to $1.8 \pm 0.5 km^3$; older than 108
905 ka) affected the Basal edifice, and the north-eastern avalanche (0.2 ± 0.1 to $1.1 \pm$
906 $0.1 km^3$; 108 – 65 ka) affected the Upper lava flow succession.

907

908 **7. ACKNOWLEDGEMENT**

909 The results presented in this work are the result of a long-lasting Ecuadorian French
910 cooperation program, carried out between the Instituto Geofísico de la Escuela
911 Politécnica Nacional (IG-EPN) through SENPLADES project (Generación de
912 Capacidades para la Emisión de Alertas Tempranas), and the Institut de Recherche
913 pour le Développement (IRD, France) through a “Laboratoire Mixte International”
914 program entitled “Séismes et Volcans dans les Andes du Nord”. We deeply thank
915 the anonymous reviewers and the Invited Editor, C. Vallejo, for their insightful
916 comments that improve the manuscript.

917

918 **8. REFERENCES**

919

920 Alvarado, A., Audin, L., Nocquet, J. M., Jaillard, E., Mothes, P., Jarrín, P., Cisneros, D., 2016.

921 Partitioning of oblique convergence in the Northern Andes subduction zone: Migration history and
922 the present-day boundary of the North Andean Sliver in Ecuador. *Tectonics*, 35(5), 1048-1065.

923 Ancellin, M. A., Samaniego, P., Vlastélic, I., Nauret, F., Gannoun, A., Hidalgo, S., 2017. Across-arc
924 versus along-arc Sr-Nd-Pb isotope variations in the E Ecuadorian volcanic arc. *Geochemistry,*
925 *Geophysics, Geosystems*, 18(3), 1163-1188.

926 Andrade, S. D., van Wyk de Vries, B., & Robin, C., 2019. Imbabura volcano (Ecuador): The influence
927 of dipping-substrata on the structural development of composite volcanoes during strike-slip
928 faulting. *Journal of Volcanology and Geothermal Research*, 385, 68-80.

929 Andrade, S. D., Müller, A. V., Vasconez, F. J., Beate, B., Aguilar, J., Santamaría, S., 2021. Pululahua
930 dome complex, Ecuador: eruptive history, total magma output and potential hazards. *Journal of*
931 *South American Earth Sciences*, 106, 103046.

932 Bablon, M., 2018. Reconstruction de l'histoire des volcans de l'arc équatorien: contraintes pour
933 l'évolution chronologique de l'arc andin et pour l'évaluation du risque volcanique (Doctoral
934 dissertation, Paris Saclay).

935 Bablon, M., Quidelleur, X., Samaniego, P., Le Pennec, J. L., Audin, L., Jomard, H., Alvarado, A.,
936 2019. Interactions between volcanism and geodynamics in the southern termination of the
937 Ecuadorian arc. *Tectonophysics*, 751, 54-72.

938 Bablon, M., Quidelleur, X., Samaniego, P., Le Pennec, J. L., Lahitte, P., Liorzou, C., Hidalgo, S.,
939 2018. Eruptive chronology of Tungurahua volcano (Ecuador) revisited based on new K-Ar ages
940 and geomorphological reconstructions. *Journal of Volcanology and Geothermal Research*, 357,
941 378-398.

942 Bablon, M., Quidelleur, X., Samaniego, P., Le Pennec, J. L., Santamaría, S., Liorzou, C., Eschbach,
943 B., 2020. Volcanic history reconstruction in northern Ecuador: insights for eruptive and erosion
944 rates on the whole Ecuadorian arc. *Bulletin of Volcanology*, 82(1), 1-23.

945 Baize, S., Audin, L., Alvarado, A., Jomard, H., Bablon, M., Champenois, J., Le Pennec, J. L., 2020a.
946 Active 961 Tectonics and Earthquake Geology Along the Pallatanga Fault, Central Andes of
947 Ecuador. *Frontiers in Earth Science*, 8, 193.

948 Baize, S., Nurminen, F., Sarmiento, A., Dawson, T., Takao, M., Scotti, O., Civico, R., 2020b. A
949 worldwide and Unified Database of Surface Ruptures (SURE) for fault displacement hazard
950 analyses. *Seismological Research Letters*, 91(1), 499-520.

951 Barberi, F., Coltelli, M., Ferrara, G., Innocenti, F., Navarro, J. M., Santacroce, R., 1988. Plio-
952 quaternary volcanism in Ecuador. *Geological Magazine*, 125(1), 1-14.

953 Beauval, C., Yepes, H., Bakun, W. H., Egred, J., Alvarado, A., Singaicho, J. C., 2010. Locations and
954 magnitudes of historical earthquakes in the Sierra of Ecuador (1587–1996). *Geophysical Journal*
955 *International*, 181(3), 1613-1633.

956 Bellver-Baca, M. T., Chiaradia, M., Beate, B., Beguelin, P., Deriaz, B., Mendez-Chazarra, N.,
957 Villagómez, D., 2020. Geochemical evolution of the Quaternary Chachimbiro Volcanic Complex
958 (frontal volcanic arc of Ecuador). *Lithos*, 356, 105237.

959 Bernard, B., & Andrade, D. (2011). Volcanes cuaternarios del Ecuador continental. *IGEPN Poster*
960 *Informativo*.

961 Bernard, B., Hidalgo, S., Robin, C., Beate, B., Quijozaca, J., 2014. The 3640–3510 BC rhyodacite
962 eruption of Chachimbiro compound volcano, Ecuador: a violent directed blast produced by a
963 satellite dome. *Bulletin of Volcanology*, 76(9), 1-20.

964 Boland, M.P., McCourt, W.J., Beate, B., 2000. Mapa geológico de la Cordillera Occidental del
965 Ecuador entre 08–s18N, escala 1/200.000. British Geological Survey-CODIGEM, Dirección
966 Nacional de Geología, Quito.

967 Bourgois, J., 2013. A review on tectonic record of strain buildup and stress release across the Andean
968 forearc along the gulf of Guayaquil-Tumbes basin (GGTB) near Ecuador-Peru
969 border. *International Journal of Geosciences*, 4, 618-635.

970 Cassagnol, C., Gillot, P.-Y., 1982. Range and effectiveness of unspiked potassium-argon dating:
971 experimental groundwork and application. *Odin GS Ed Numer. Dating Stratigr.* John Wiley & Sons,
972 New York, 159–179.

973 Clapperton, C. M., 1990. Glacial and volcanic geomorphology of the Chimborazo-Carihuairazo
974 massif, Ecuadorian Andes. *Earth and Environmental Science Transactions of the Royal Society*
975 *of Edinburgh*, 81(2), 91-116.

976 Cole, J. W., Milner, D. M., Spinks, K. D., 2005. Calderas and caldera structures: a review. *Earth-*
977 *Science Reviews*, 69(1-2), 1-26.

978 Cotten, J., Le Dez, A., Bau, M., Caroff, M., Maury, R. C., Dulski, P., Brousse, R., 1995. Origin of
979 anomalous rare-earth element and yttrium enrichments in subaerially exposed basalts: evidence
980 from French Polynesia. *Chemical Geology*, 119(1-4), 115-138.

981 Deino, A., Potts, R., 1992. Age-probability spectra for examination of single-crystal $^{40}\text{Ar}/^{39}\text{Ar}$ dating
982 results: Examples from Olorgesailie, southern Kenya Rift. *Quaternary International*, 13, 47-53.

983 Deligne, N. I., Coles, S. G., Sparks, R. S. J., 2010. Recurrence rates of large explosive volcanic
984 eruptions. *Journal of Geophysical Research: Solid Earth*, 115(B6).

985 Deline, P. (2009). Interactions between rock avalanches and glaciers in the Mont Blanc massif during
986 the late Holocene. *Quaternary Science Reviews*, 28(11-12), 1070-1083.

987 Dibacto Kamwa, S., 2020. Dynamique de construction et démantèlement des volcans tertiaires et
988 quaternaires des Carpates par des approches géomorphologiques et géochronologiques
989 (Doctoral dissertation, université Paris-Saclay).

990 Dufresne, A., Siebert, L., Bernard, B., 2021. Distribution and geometric parameters of volcanic debris-
991 avalanche deposits. In *Volcanic Debris Avalanches* (pp. 75-90). Springer, Cham.

992 Ego, F., Sébrier, M., Carey-Gailhardis, E., Beate, B., 1996. Do the Billecocha normal faults (Ecuador)
993 reveal extension due to lithospheric body forces in the northern Andes?. *Tectonophysics*, 265(3-
994 4), 255-273.

995 Ego, F., Sébrier, M., Lavenu, A., Yepes, H., Egues, A., 1996. Quaternary state of stress in the
996 Northern Andes and the restraining bend model for the Ecuadorian
997 Andes. *Tectonophysics*, 259(1-3), 101-116.

998 Eguez, A., Alvarado, A., Yepes, H., Machette, M. N., Costa, C., Dart, R. L., Bradley, L. A., 2003.
999 Database and map of Quaternary faults and folds of Ecuador and its offshore regions. US
1000 Geological Survey Open-File Report, 3, 289. doi=10.1.1.593.980

1001 Feininger, T., Bristow, C. R., 1980. Cretaceous and Paleogene geologic history of coastal
1002 Ecuador. *Geologische Rundschau*, 69(3), 849-874.

1003 Germa, A., Lahitte, P., Quidelleur, X., 2015 Construction and destruction of Mont Pelée volcano:
1004 volumes and rates constrained from a geomorphological model of evolution: construction and
1005 destruction of Mont Pelée. *J Geophys Res Earth Surf* 120:1206–1226.
1006 <https://doi.org/10.1002/2014JF003355>

1007 Germa, A., Quidelleur, X., Lahitte, P., Labanieh, S., Chauvel, C., 2011. The K–Ar Cassagnol– Gillot
1008 technique applied to western Martinique lavas: A record of Lesser Antilles arc ACCEPTED
1009 MANUSCRIPT ACCEPTED MANUSCRIPT 32 activity from 2 Ma to Mount Pelée volcanism. *Quat.*
1010 *Geochronol.* 6, 341–355.

1011 Gillot, P.-Y., Hildenbrand, A., Lefèvre, J.-C., Albore-Livadie, C., 2006. The K/Ar dating method:
1012 principle, analytical techniques, and application to Holocene volcanic eruptions in Southern Italy.
1013 *Acta Vulcanol.* 18, 55–66.

1014 Goossens, P. J., Rose Jr, W. I., 1973. Chemical composition and age determination of tholeiitic rocks
1015 in the basic igneous complex, Ecuador. *Geological Society of America Bulletin*, 84(3), 1043-1052.

1016 Guillier, B., Chatelain, J. L., Jaillard, E., Yepes, H., Poupinet, G., Fels, J. F., 2001. Seismological
1017 evidence on the geometry of the orogenic system in central-northern Ecuador (South
1018 America). *Geophysical Research Letters*, 28(19), 3749-3752.

1019 Gunkel, G., Beulker, C., 2009. Limnology of the Crater Lake Cuicocha, Ecuador, a cold-water tropical
1020 lake. *International Review of Hydrobiology*, 94(1), 103-125.

1021 Gunkel, G., Beulker, C., Grupe, B., Viteri, F., 2009. Survey and assessment of post volcanic activities
1022 of a young caldera lake, Lake Cuicocha, Ecuador. *Natural Hazards and Earth System*
1023 *Sciences*, 9(3), 699.

1024 Gutscher, M.-A., J., Malavieille, S., Lallemand., J.-Y., Collot, 1999, Tectonic segmentation of the
1025 North Andean margin: Impact of the Carnegie Ridge collision, *Earth Planet. Sci. Lett.*, 168(3), 255–
1026 270.

- 1027 Hall, M. L., Mothes, P. A., 1994. Tefroestratigrafía holocénica de los volcanes principales del valle
1028 interandino, Ecuador. *Estudios de geografía*, 6, 47-67.
- 1029 Hall, M. L., & Wood, C. A. (1985). Volcano-tectonic segmentation of the northern Andes. *Geology*,
1030 13(3), 203-207.
- 1031 Hall, M. L., Mothes, P. A., Samaniego, P., Militzer, A., Beate, B., Ramón, P., Robin, C., 2017. Antisana
1032 volcano: a representative andesitic volcano of the eastern cordillera of Ecuador: petrography,
1033 chemistry, tephra, and glacial stratigraphy. *Journal of South American Earth Sciences*, 73, 50-64.
- 1034 Hall, M. L., Robin, C., Beate, B., Mothes, P., Monzier, M., 1999. Tungurahua Volcano, Ecuador:
1035 structure, eruptive history, and hazards. *Journal of Volcanology and Geothermal Research*, 91(1),
1036 1-21.
- 1037 Hall, M. L., Samaniego, P., Le Pennec, J. L., Johnson, J. B., 2008. Ecuadorian Andes volcanism: A
1038 review of Late Pliocene to present activity. *Journal of Volcanology and Geothermal
1039 Research*, 176(1), 1-6.
- 1040 Hall, M., Mothes, P., 2008. The rhyolitic–andesitic eruptive history of Cotopaxi volcano,
1041 Ecuador. *Bulletin of Volcanology*, 70(6), 675-702.
- 1042 Hall, M., Ramón, P., Mothes, P., Le Pennec, J. L., García, A., Samaniego, P., Yepes, H., 2004.
1043 Volcanic eruptions with little warning: the case of Volcán Reventador's Surprise November 3, 2002
1044 Eruption, Ecuador. *Revista geológica de Chile*, 31(2), 349-358.
- 1045 Harford, C.L., Pringle, M.S., Sparks, R.S.J., Young, S.R., 2002. The volcanic evolution of Montserrat
1046 using $^{40}\text{Ar}/^{39}\text{Ar}$ geochronology. *Geol. Soc. Lond. Mem.* 21, 93–113.
- 1047 Hidalgo, S., Gerbe, M. C., Martin, H., Samaniego, P., Bourdon, E., 2012. Role of crustal and slab
1048 components in the Northern Volcanic Zone of the Andes (Ecuador) constrained by Sr–Nd–O
1049 isotopes. *Lithos*, 132, 180-192.
- 1050 Hidalgo, S., Monzier, M., Almeida, E., Chazot, G., Eissen, J. P., van der Plicht, J., Hall, M. L., 2008.
1051 Late Pleistocene and Holocene activity of the Atacazo–Ninahuilca volcanic complex
1052 (Ecuador). *Journal of Volcanology and Geothermal Research*, 176(1), 16-26.
- 1053 Hughes, R. A., Pilatasig, L. F., 2002. Cretaceous and Tertiary terrane accretion in the Cordillera
1054 Occidental of the Andes of Ecuador. *Tectonophysics*, 345(1-4), 29-48.
- 1055 Jaillard, E., Ordonez, M., Suarez, J., Toro, J., Iza, D., Lugo, W., 2004. Stratigraphy of the Late
1056 Cretaceous–Paleogene deposits of the cordillera occidental of central Ecuador: geodynamic
1057 implications. *Journal of South American Earth Sciences*, 17(1), 49-58.
- 1058 Jomard, H., Saqui, D., Baize, S., Alvarado, A., Bernard, B., Audin, L., Hidalgo, S., Pacheco, D., Ruiz,
1059 M., Segovia, M., 2021. Interactions between active tectonics and gravitational deformation along
1060 with the Billecocha fault system (Northern Ecuador): Insights from morphological and
1061 paleoseismological investigations, *Journal of South American Earth Sciences*. DOI: [HTTPS://
1062 doi.org/10.1016/j.jsames.2021.103406](https://doi.org/10.1016/j.jsames.2021.103406).

1063 Kerr, A. C., Aspden, J. A., Tarney, J., Pilatasig, L. F., 2002. The nature and provenance of accreted
1064 oceanic terranes in western Ecuador: geochemical and tectonic constraints. *Journal of the*
1065 *Geological Society*, 159(5), 577-594.

1066 Lahitte, P., Samper, A., Quidelleur, X., 2012. DEM-based reconstruction of southern Basse-Terre
1067 volcanoes (Guadeloupe archipelago, FWI): Contribution to the Lesser Antilles Arc construction
1068 rates and magma production. *Geomorphology*, 136(1), 148-164.

1069 Lara, L. E., 2009. The 2008 eruption of the Chaitén Volcano, Chile: a preliminary report. *Andean*
1070 *Geology*, 36(1), 125-129.

1071 Le Pennec, J. L., Ruiz, A. G., Eissen, J. P., Hall, M. L., Fornari, M., 2011. Identifying potentially active
1072 volcanoes in the Andes: Radiometric evidence for late Pleistocene-early Holocene eruptions at
1073 Volcán Imbabura, Ecuador. *Journal of Volcanology and Geothermal Research*, 206(3-4), 121-
1074 135.

1075 Legros, F., 2000. Minimum volume of a tephra fallout deposit estimated from a single isopach. *Journal*
1076 *of Volcanology and Geothermal Research*, 96(1-2), 25-32.

1077 Lipman, P. W. (2000). Calderas. *Encyclopedia of volcanoes*, 643-662.

1078 Lonsdale, P., 2005. Creation of the Cocos and Nazca plates by fission of the Farallon plate,
1079 *Tectonophysics*, 404(3-4), 237–264, doi:10.1016/j.tecto.2005.05.011.

1080 Luzieux, L. D. A., Heller, F., Spikings, R., Vallejo, C. F., Winkler, W., 2006. Origin and Cretaceous
1081 tectonic history of the coastal Ecuadorian forearc between 1 N and 3 S: Paleomagnetic,
1082 radiometric and fossil evidence. *Earth and Planetary Science Letters*, 249(3-4), 400-414.

1083 Madera, L. F., 1918. Ibarra y el terremoto de 1868.

1084 Melián, G. V., Toulkeridis, T., Pérez, N. M., Hernández, P. A., Somoza, L., Padrón, E., Cordero, M.,
1085 2021. Geochemistry of Water and Gas Emissions from Cuicocha and Quilotoa Volcanic Lakes,
1086 Ecuador. *Front. Earth Sci*, 9, 741528.

1087 Michaud, F., C. Witt., J. Y. Royer., 2009, Influence of the subduction of the Carnegie volcanic ridge
1088 on Ecuadorian geology: Reality and fiction, *Geol. Soc. Jpn. Mem.*, 204, 217–228,
1089 doi:10.1130/2009.1204(10).

1090 Monzier, M., Robin, C., Samaniego, P., Hall, M. L., Cotten, J., Mothes, P., Arnaud, N., 1999. Sangay
1091 volcano, Ecuador: structural development, present activity, and petrology. *Journal of Volcanology*
1092 *and Geothermal Research*, 90(1-2), 49-79.

1093 Navarrete, W.F., Le Pennec, J.L., Solano, S., Liorzou, C., Ruiz, G.A., 2020. A first reconstruction of
1094 the evolution of Cubilche Volcanic complex, Imbabura Province, Ecuador. *J. Volcanol. Geotherm.*
1095 *Res.* 406, 107023 <https://doi.org/10.1016/j.jvolgeores.2020.107023>.

1096 Newhall, C. G., & Punongbayan, R. (Eds.), 1996. Fire and mud: eruptions and lahars of Mount
1097 Pinatubo, Philippines (p. 1126). Quezon City: Philippine Institute of Volcanology and Seismology.

1098 Newhall, C.G., Self, S., 1982. The volcanic explosivity index (VEI) an estimate of explosive magnitude
1099 for historical volcanism. *J. Geophys. Res.: Oceans* 87, 1231–1238.

1100 Nocquet, J. M., Villegas-Lanza, J. C., Chlieh, M., Mothes, P. A., Rolandone, F., Jarrin, P., Yepes, H.,
1101 2014. Motion of continental slivers and creeping subduction in the northern Andes. *Nature*
1102 *Geoscience*, 7(4), 287-291.

1103 Peccerillo, A., Taylor, S.R., 1976. Geochemistry of Eocene calc-alkaline volcanic rocks from the
1104 Kastamonu area, northern Turkey. *Contrib. Mineral. Petrol.* 58, 63–81.

1105 Picuasi, S., Julio, C. 2013. Aportes al Ordenamiento Territorial desde la cosmovisión de los pueblos
1106 originarios (Bachelor's thesis).

1107 Pidgen, A., 2014. Cuicocha Volcano, Ecuador: reconstruction of major explosive phases through
1108 investigation of associated pyroclastic deposits. Trinity: University of Oxford (Master's thesis).

1109 Pratt, W. T., Duque, P., Ponce, M., 2005. An autochthonous geological model for the eastern Andes
1110 of Ecuador. *Tectonophysics*, 399(1-4), 251-278.

1111 Punongbayan, R. S., Newhall, C. G., Hoblitt, R. P., 1996. Photographic record of rapid geomorphic
1112 change at Mount Pinatubo, 1991–94. *Fire and Mud: Eruptions and Lahars of Mount Pinatubo,*
1113 *Philippines*, 21-66.

1114 Reimer, P. J. 2020. Composition and consequences of the IntCal20 radiocarbon calibration curve.
1115 *Quaternary Research*, 96, 22-27.

1116 Reimer, P. J., Bard, E., Bayliss, A., Beck, J. W., Blackwell, P. G., Ramsey, C. B., Van Der Plicht, J.,
1117 2013. IntCal13 and Marine13 radiocarbon age calibration curves 0–50,000 years cal
1118 BP. *radiocarbon*, 55(4), 1869-1887.

1119 Ricci, J., Lahitte, P., Quidelleur, X., 2015a. Construction and destruction rates of volcanoes within
1120 tropical environment: Examples from the Basse-Terre Island (Guadeloupe, Lesser Antilles).
1121 *Geomorphology* 228, 597–607.

1122 Ricci, J., Quidelleur, X., Lahitte, P., 2015b. Volcanic evolution of central Basse-Terre Island revisited
1123 on the basis of new geochronology and geomorphology data. *Bull. Volcanol.* 77.

1124 Robin, C., Samaniego, P., Le Pennec, J. L., Fornari, M., Mothes, P., Van Der Plicht, J., 2010. New
1125 radiometric and petrological constraints on the evolution of the Pichincha volcanic complex
1126 (Ecuador). *Bulletin of volcanology*, 72(9), 1109-1129.

1127 Robin, C., Samaniego, P., Le Pennec, J.L., Fornari, M., Mothes, P., van der Plicht, J., 2010. New
1128 radiometric and petrological constraints on the evolution of the Pichincha volcanic complex
1129 (Ecuador). *Bull. Volcanol.* 72, 1109–1129. <http://dx.doi.org/10.1007/s00445-010-0389-0>

1130 Roverato, M., Dufresne, A., Procter, J., 2021. Volcanic Debris Avalanches.

1131 Roverato, M., Larrea, P., Casado, I., Mulas, M., Béjar, G., Bowman, L., 2018. Characterization of the
1132 Cubilche debris avalanche deposit, a controversial case from the northern Andes,
1133 Ecuador. *Journal of Volcanology and Geothermal Research*, 360, 22-35.

1134 Samaniego, P., Barba, D., Robin, C., Fornari, M., Bernard, B., 2012. Eruptive history of Chimborazo
1135 volcano (Ecuador): A large, ice-capped and hazardous compound volcano in the Northern
1136 Andes. *Journal of Volcanology and Geothermal Research*, 221, 33-51.

1137 Samaniego, P., Martin, H., Monzier, M., Robin, C., Fornari, M., Eissen, J. P., Cotten, J., 2005.
1138 Temporal evolution of magmatism in the Northern Volcanic Zone of the Andes: the geology and
1139 petrology of Cayambe Volcanic Complex (Ecuador). *Journal of petrology*, 46(11), 2225-2252.

1140 Samaniego, P., Monzier, M., Robin, C., Hall, M. L., 1998. Late Holocene eruptive activity at Nevado
1141 Cayambe Volcano, Ecuador. *Bulletin of Volcanology*, 59(7), 451-459.

1142 Samaniego, P., Rivera, M., Mariño, J., Guillou, H., Liorzou, C., Zerathe, S., Scao, V., 2016. The
1143 eruptive chronology of the Ampato–Sabancaya volcanic complex (Southern Peru). *Journal of*
1144 *Volcanology and Geothermal Research*, 323, 110-128.

1145 Samaniego, P., Ordóñez, J., Bablon, M., Hall, M. L., Quidelleur, X., Lahitte, P., Liorzou, C., 2022. The
1146 eruptive chronology of the Carihuairazo volcano (Ecuador): Recurrent sector collapses of a Middle
1147 Pleistocene stratovolcano of the northern andes. *Journal of South American Earth Sciences*, 116,
1148 103865.

1149 Samper, A., Quidelleur, X., Lahitte, P., Mollex, D., 2007. Timing of effusive volcanism and collapse
1150 events within an oceanic arc island: Basse-Terre, Guadeloupe archipelago (Lesser Antilles Arc).
1151 *Earth Planet. Sci. Lett.* 258, 175–191.

1152 Satake, K., Kate, Y., 2001. The 1741 Oshima-Oshima eruption: extent and volume of submarine
1153 debris avalanche. *Geophys Res Lett* 28(3):427–430

1154 Sierra, D., Hidalgo, S., Almeida, M., Vigide, N., Lamberti, M. C., Proaño, A., Narváez, D. F., 2021.
1155 Temporal and spatial variations of CO₂ diffuse volcanic degassing on Cuicocha Caldera Lake–
1156 Ecuador. *Journal of Volcanology and Geothermal Research*, 411, 107145.

1157 Singer, B. S., Wijbrans, J. R., Nelson, S. T., Pringle, M. S., Feeley, T. C., Dungan, M. A., 1998.
1158 Inherited argon in a Pleistocene andesite lava: ⁴⁰Ar/³⁹Ar incremental-heating and laser-fusion
1159 analyses of plagioclase. *Geology*, 26(5), 427-430.

1160 Spikings, R. A., Winkler, W., Hughes, R. A., Handler, R., 2005. Thermochronology of allochthonous
1161 terranes in Ecuador: Unravelling the accretionary and post-accretionary history of the Northern
1162 Andes. *Tectonophysics*, 399(1-4), 195-220.

1163 Stuiver, M., Reimer, P. J., 1993. Extended 14C database and revised CALIB radiocarbon calibration
1164 program, *Radiocarbon* 35, 215-230.

1165 Stuiver, M., Reimer, P.J., Reimer, R.W., 2005. CALIB 5.0. [WWW program and documentation].

1166 Sun, S.-s., McDonough, W.F., 1989. Chemical and isotopic systematics of oceanic basalts:
1167 implications for mantle composition and processes. *Geol. Soc. Lond. Spec. Publ.* 42, 313–345.

1168 Thouret, J.C., Finizola, A., Fornari, M., Suni, J., Legeley-Padovani, A., Frechen, M., 2001. Geology
1169 of El Misti volcano nearby the city of Arequipa, Peru. *Geol. Soc. Am. Bull.* 113, 1593–1610

1170 Trenkamp, R., Kellogg, J. N., Freymueller, J. T., Mora, H. P., 2002. Wide plate margin deformation,
1171 southern Central America and northwestern South America, CASA GPS observations. *Journal of*
1172 *South American Earth Sciences*, 15(2), 157-171.

1173 Troya, R., 1913. Photo from the historical archive of the Central Bank of Ecuador. *Quito, Ecuador.*
1174 *Code*, 95, F0490.

1175 Troya, R., 1913. Photo from the historical archive of the Central Bank of Ecuador. *Quito, Ecuador.*
1176 *Code, 95, F0490.*

1177 UN/ISDR ISfDR., 2004. Living with risk: A global review of disaster reduction initiatives, vol 1. United
1178 Nations Publications, New York and Geneva, URL http://www.unisdr.org/files/657_lwr1.pdf

1179 Vallejo Vargas, S. X., 2011. *Distribución de las cenizas volcánicas Holocénicas Tardías en la Costa*
1180 *del Ecuador* (Bachelor's thesis, QUITO/EPN/2011).

1181 Vallejo, C., Almagor, S., Romero, C., Herrera, J. L., Escobar, V., Spikings, R. A., Vermeesch, P.,
1182 2020. Sedimentology, provenance and radiometric dating of the Silante Formation: Implications
1183 for the Cenozoic evolution of the Western Andes of Ecuador. *Minerals*, 10(10), 929.

1184 Vallejo, C., Spikings, R. A., Horton, B. K., Luzieux, L., Romero, C., Winkler, W., Thomsen, T. B., 2019.
1185 Late Cretaceous to Miocene stratigraphy and provenance of the coastal forearc and Western
1186 Cordillera of Ecuador: Evidence for accretion of a single oceanic plateau fragment. In *Andean*
1187 *tectonics* (pp. 209-236). Elsevier.

1188 Vallejo, C., Spikings, R. A., Luzieux, L., Winkler, W., Chew, D., Page, L., 2006. The early interaction
1189 between the Caribbean Plateau and the NW South American Plate. *Terra Nova*, 18(4), 264-269.

1190 Vallejo, C., Winkler, W., Spikings, R. A., Luzieux, L., Heller, F., Bussy, F., 2009. Mode and timing
1191 of terrane accretion in the forearc of the Andes in Ecuador. *Backbone of the Americas: shallow*
1192 *subduction, plateau uplift, and ridge and terrane collision*, 204, 197.

1193 Valverde, V., Mothes, P. A., Beate, B., Bernard, J., 2021. Enormous and far-reaching debris
1194 avalanche deposits from Sangay volcano (Ecuador): Multidisciplinary study and modeling the 30-
1195 ka sector collapse. *Journal of Volcanology and Geothermal Research*, 411, 107172.

1196 Van Thournout, F., Hertogen, J., Quevedo, L., 1992. Allochthonous terranes in northwestern
1197 Ecuador. *Tectonophysics*, 205(1-3), 205-221.

1198 Váscquez Müller, A., Cashman, K.V., Mitchell, S.J., Váscquez, F.J., 2022. The 2.6–2.3 ka explosive
1199 eruptive period of the Pululahua dome complex, Ecuador: insights from pyroclast analysis. *Bull*
1200 *Volcanol* 84:81. <https://doi.org/10.1007/s00445-022-01590-4>

1201 Voight, B., Glicken, H., Janda, R. J., Douglass, P. M., 1981. Catastrophic rockslide avalanche of May
1202 18. In: Lipman P.W., Mullineaux D.R. (eds) *The 1980 eruptions of Mount St. Helens*, Washington,
1203 U.S. Geological Survey Professional Papers 1250:347–377

1204 Von Hillebrandt, C., 1989. Estudio geovolcanológico del Complejo Volcánico Cuicocha-Cotacachi y
1205 sus aplicaciones. Provincia de Imbabura. Quito: Escuela Politécnica Nacional (Master's thesis).

1206 Von Hillebrandt, C., Hall, M. L., 1988. Mapa de los Peligros Volcánicos Potenciales Asociados con
1207 el Volcán Cuicocha. *Esc*, 1(50.000).

1208 Whympers, E., 1892. *Travels amongst the Great Andes of the Equator* (Vol. 1). C. Scribner's Sons.

1209 Wilson, M., 1989. Igneous petrogenesis. A global tectonic approach. Chapman and Hall, London,
1210 Glasgow, New York, Tokyo, Melbourne, Madras., pp. 51-97. ISBN: 0-412-53310-3

1211 Wolf, T., 1892. Geografía y geología del Ecuador; publicada por orden del supremo gobierno de la
1212 república por Teodoro Wolf. Tipografía de FA Brockhaus.

1213 Yepes, H., Audin, L., Alvarado, A., Beauval, C., Aguilar, J., Font, Y., Cotton, F., 2016. A new view for
1214 the geodynamics of Ecuador: Implication in seismogenic source definition and seismic hazard
1215 assessment. *Tectonics*, 35(5), 1249-1279.

1216

1217

1218

1219

1220

1221

1222

1223

1224

1225

1226

1227

1228

1229

1230

1231

1232

1233

1234

1235

1236

1237

1238

1239

1240

1241

1242

1243

1244

1245

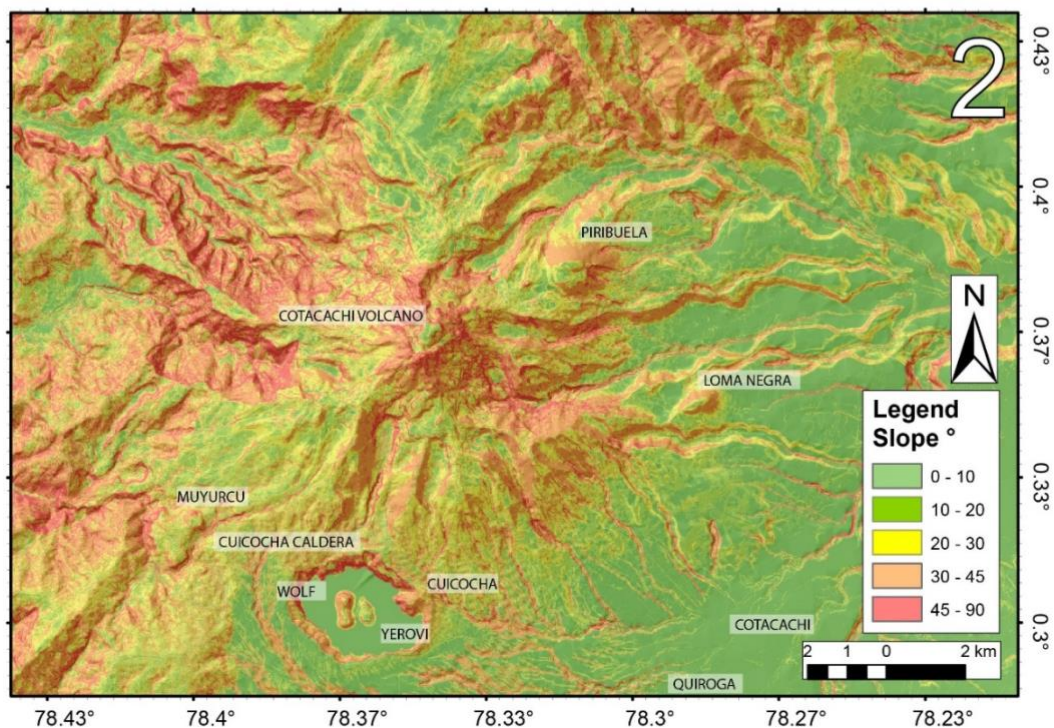
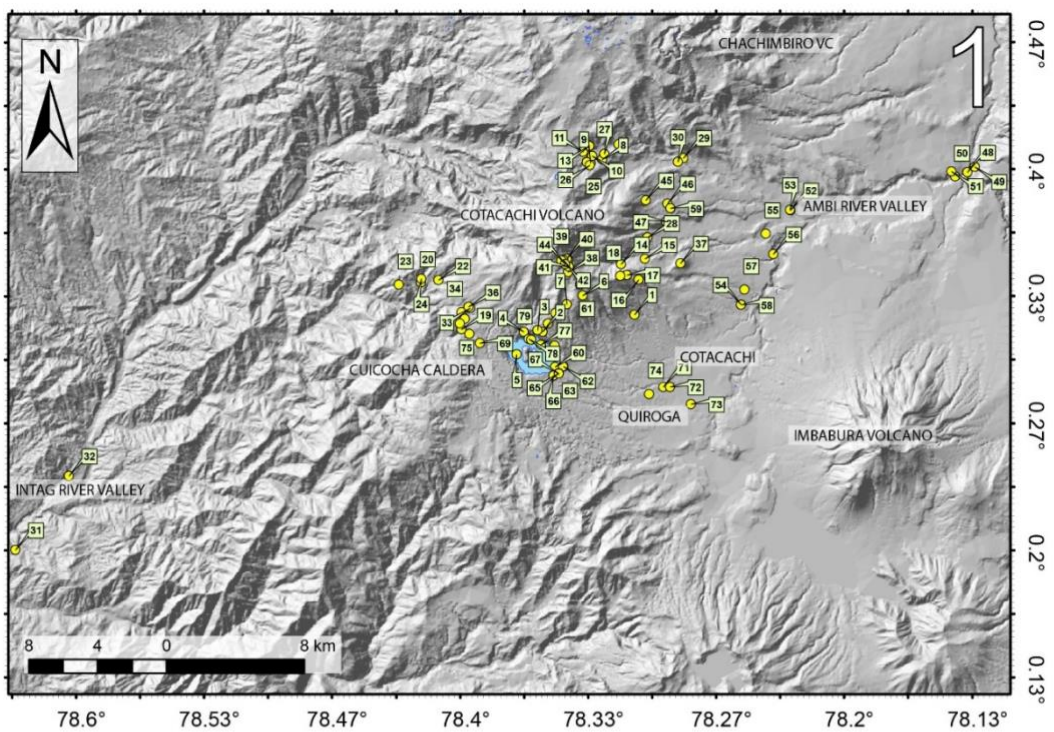
1246

1247

1248

1249

1250



1252

1253

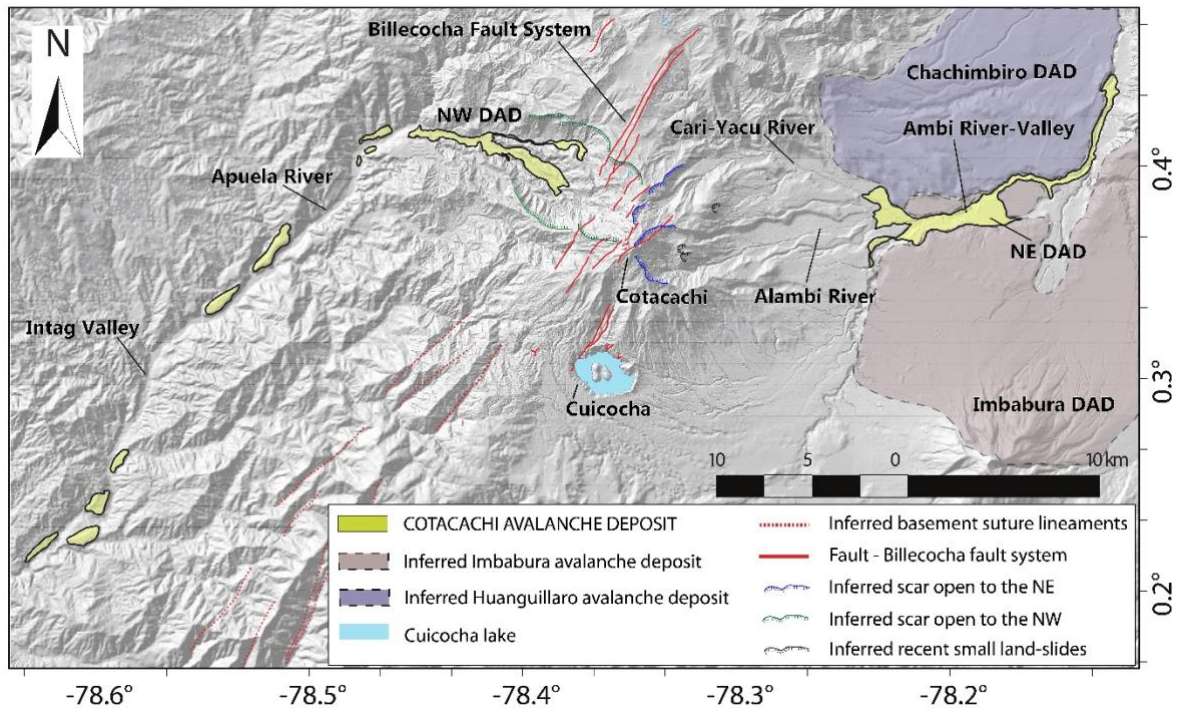
1254

1255

1256

Figure A 1) Field control points of Cotacachi - Cuicocha volcanic complex, for detailed descriptions of each number, see: Table A. 2) Map of slopes of the area of the Cotacachi - Cuicocha volcanic complex. The map was made using five classes based on the angles of inclination of the slope, expressed in degrees (°).

1257



1258

1259

1260

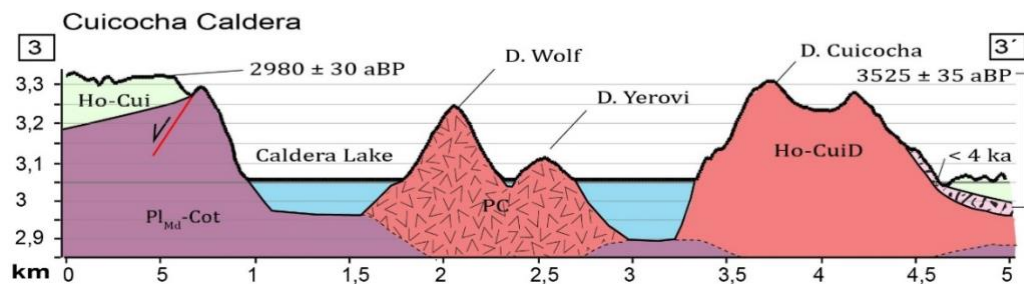
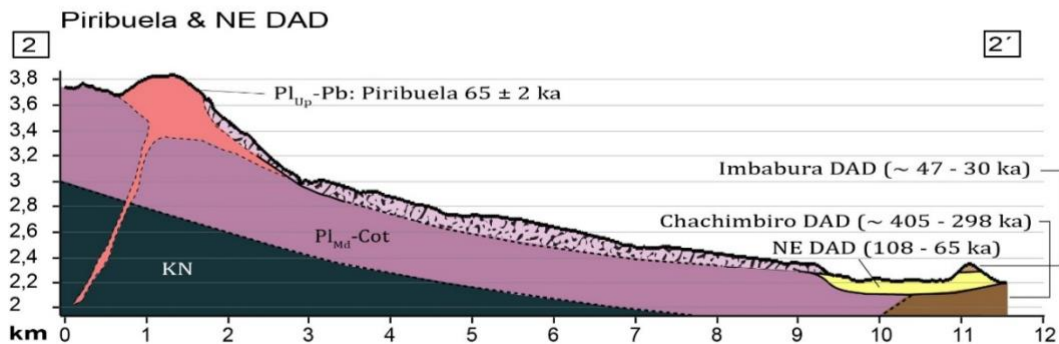
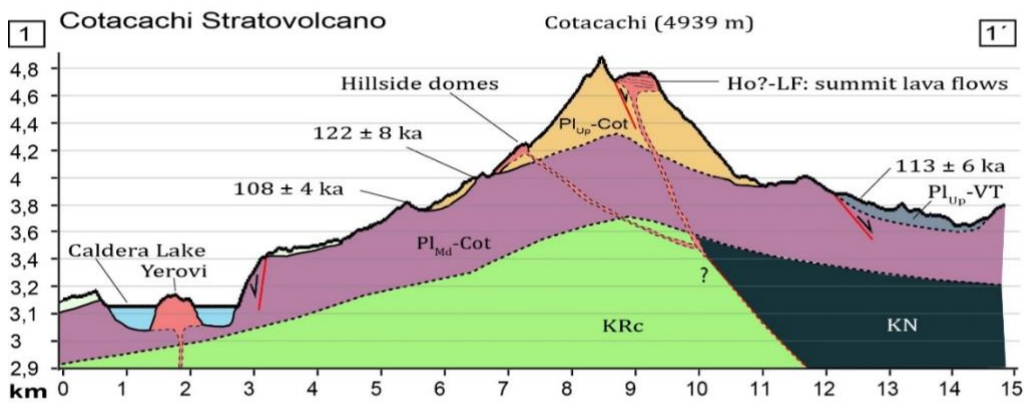
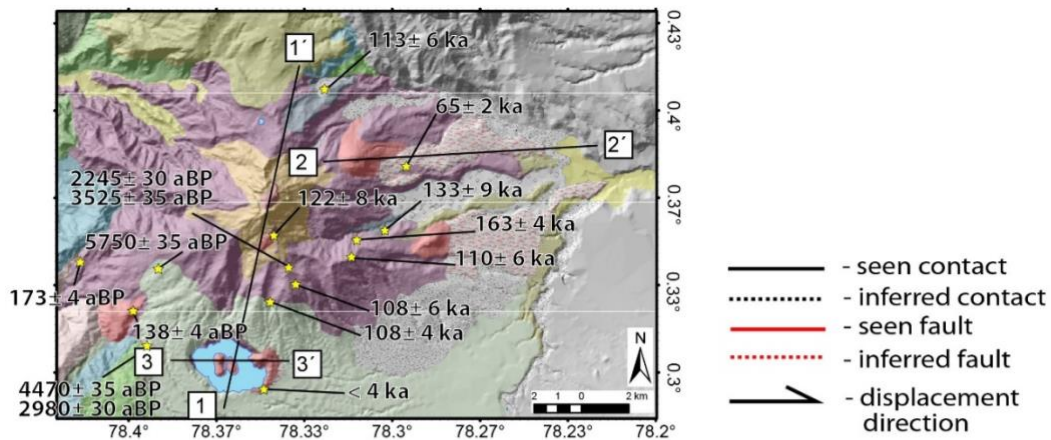
1261

1262

1263

1264

Figure B. Spatial distribution of the mapped NW and NE avalanche deposits (yellow-colored areas) and possible avalanche scars. Note the Billecocha fault system (Ego, 1996; Egeuz et al., 2003; Jomard et al., 2021) crossing the center of the possible avalanche scars. Purple and light brown polygons show the boundaries of the Chachimbiro and Imbabura avalanches. The inferred basement suture lineaments were taken from Boland et al. (2000).



1265

1266

1267

1268

1269

1270

1271

Figure C. Geological profiles show the spatial distribution of the different stratigraphic members and units. The profiles are adjusted to the observations made during the fieldwork and are consistent with the radiometric and radiocarbon ages obtained during the present study. 1) Profile 1-1': NNE-SSW longitudinal section along Cotacachi and Cuicocha. 2) Profile 2-2': Section W-E shows the spatial arrangement of the recent deposits of Piribuela and the avalanche deposits of Cotacachi, Imbabura, and Chachimbiro. 3) Profile 3-3': Section W-E of the Caldera de Cuicocha.